

Theory of 2D superconductor with broken inversion symmetry

Ol'ga Dimitrova

*L.D.Landau Institute for Theoretical Physics, Moscow, 119334, Russia and
The Abdus Salam International Center for Theoretical Physics, Strada Costiera 11, 34100 Trieste, Italy*

M. V. Feigel'man

L.D.Landau Institute for Theoretical Physics, Moscow, 119334, Russia

(Dated: April 20, 2022)

A detailed theory of a phase diagram of a 2D surface superconductor in a parallel magnetic field is presented. A spin-orbital interaction of the Rashba type is known⁴ to produce at a high magnetic field h (and in the absence of impurities) an inhomogeneous superconductive phase similar to the Larkin-Ovchinnikov-Fulde-Ferrel (LOFF) state with an order parameter $\Delta(\mathbf{r}) \propto \cos(\mathbf{Q}\mathbf{r})$. We consider the case of a strong Rashba interaction with the spin-orbital splitting much larger than the superconductive gap Δ , and show that at low temperatures $T \leq 0.4T_{c0}$ the LOFF-type state is separated from the usual homogeneous state by a first-order phase transition line. At higher temperatures another inhomogeneous state with $\Delta(\mathbf{r}) \propto \exp(i\mathbf{Q}\mathbf{r})$ intervenes between the uniform BCS state and the LOFF-like state at $g\mu_B h \approx 1.5T_{c0}$. The modulation vector Q in both phases is of the order of $g\mu_B h/v_F$. The superfluid density n_s^{yy} vanishes in the region around the second-order transition line between the BCS state and the new “helical” state. Non-magnetic impurities suppress both inhomogeneous states, and eliminate them completely at $T_{c0}\tau \leq 0.11$. However, once an account is made of the next-order term over the small parameter $\alpha/v_F \ll 1$, a relatively long-wave helical modulation with $Q \sim g\mu_B h\alpha/v_F^2$ is found to develop from the BCS state. This long-wave modulation is stable with respect to disorder. In addition, we predict that unusual vortex defects with a continuous core exist near the phase boundary between the helical and the LOFF-like states. In particular, in the LOFF-like state these defects may carry a half-integer flux.

PACS numbers: 74.20.Rp, 74.25.Dw

I. INTRODUCTION

There are experimental indications¹ in favor of existence of superconductive states localized on a surface of non-superconductive (or even insulating) bulk material. Such a superconductive state should possess a number of unusual features due to the absence of the symmetry “up” v/s “down” near the surface: the condensate wave-function is neither singlet nor triplet, but a mixture of both^{2,3}; the Pauli susceptibility is enhanced at low temperatures³ (as compared with the usual superconductors); the paramagnetic breakdown of the superconductivity in a parallel magnetic field is moved towards much higher field values due to a formation of an inhomogeneous superconductive state⁴ similar to the one predicted by Larkin-Ovchinnikov and Fulde-Ferrel^{5,6} (LOFF) for a ferromagnetic superconductor. All these features steam from the chiral subband splitting of the free electron spectrum at the surface, due to the presence of the spin-orbital Rashba term⁷; the magnitude of this splitting αp_F is small compared to the Fermi energy but can be rather large with respect to other energies in the problem. The line of transition from normal to (any of) superconductive state $T_c(h)$ was determined in [4]; however, the nature of the transition between the usual homogeneous (BCS) superconductive state at low fields and the LOFF-like state at high fields was not studied.

In this paper we provide a detailed study of the phase diagram of a surface superconductor in a parallel magnetic field h (a brief account of our results was pub-

lished in Ref. 8). We show that at moderate values of $h \sim T_c/\mu_B$ the behavior of this system is rather different from 2D LOFF model of [9]. Namely, we demonstrate the existence of a *short-wavelength* helical state with an order parameter $\Delta \propto \exp(i\mathbf{Q}\mathbf{r})$ (where $\mathbf{Q} \perp \mathbf{h}$ and $Q \sim \mu_B h/v_F$) in a considerable part of the phase diagram, which is summarized in Fig. 1. The line \mathcal{LT} is the second-order transition line separating the helical state from the homogeneous superconductor. Below the \mathcal{T} point a direct first-order transition between the homogeneous and the LOFF-like state takes place. The line \mathcal{TO} shown in Fig. 1 marks the border of metastability of the BCS state; we expect that the actual first-order transition line is (slightly) shifted towards lower H values. The line \mathcal{ST}' marks the second-order transition between the helical and the LOFF-like state. The above results are valid within the leading (the zeroth-order) approximation over the small parameter $\alpha/v_F \ll 1$; an account of the terms linear in $\alpha/v_F \ll 1$ leads, in agreement with [10], to the transformation of the uniform BCS state into a *long-wavelength helical* state with a wave vector $q \sim \alpha H/v_F^2$ at the lowest magnetic fields. Therefore, the \mathcal{LT} line is actually a line of a sharp crossover (with a relative width of the order of α/v_F) between the long- and the short-wavelength phases.

The rest of the paper is organized as follows. In Sec. II we introduce a model of a spin-orbital superconductor in a parallel magnetic field, with a hierarchy of the energies $\epsilon_F \gg \alpha p_F \gg T_c$. In Sec. III we derive the Ginzburg-Landau functional for an inhomogeneous ground state.

On the $T_c(H)$ line we find two critical points: the Lifshitz point \mathcal{L} and the symmetric point \mathcal{S} , and demonstrate the existence of a “helical” state with an order parameter $\Delta(\mathbf{r}) \propto \exp(i\mathbf{Q}\mathbf{r})$ and a *large* $Q \sim H/v_F$. The point \mathcal{S} on the $T_c(H)$ line is special in the sense that there the order parameter symmetry is enhanced to $U(2)$ from the usual $U(1)$. That leads to unusual vortex textures discussed in Sec. IV. In particular, vortices with half-integer flux are predicted for the LOFF-like state. In Sec. V we derive the two stationary conditions for the helical state, which determine the equilibrium Δ and Q . The latter allows to establish the boundaries of stability of the BCS and helical state: the Lifshitz line terminating in the critical Landau point \mathcal{T} , and a line starting in the symmetric point \mathcal{S} . We show that the helical state and the parity-even (stripe) phase are separated by two phase transitions of the second order and an intervening additional superconducting phase. In Sec. VI we prove that the electric current is zero in the ground state; then we show that the supercurrent response to the vector potential component $A_y = \mathbf{A}\mathbf{Q}/Q$ vanishes at the \mathcal{LT} line, whereas within the helical state both components of the superfluid density tensor \hat{n}_s are of the same magnitude as the superfluid density in the BCS state. In Sec. VII we explore the influence upon the phase diagram of the terms linear in $\alpha/v_F \ll 1$. We show that at low magnetic fields the ground state is realized as a weakly helical state with zero current. A special geometry is proposed when an oscillating supercurrent in the ground state of the helical phase may flow. In Sec. VIII we study the effect of the non-magnetic impurities on the phase diagram. We show that in the relatively clean case the paramagnetic critical field is quickly suppressed by disorder and the position of the Lifshitz point is shifted towards higher magnetic field values. We find the critical strength of disorder above which all short-wavelength inhomogeneous states are eliminated from the phase diagram; in terms of an elastic scattering time τ this condition reads $\tau_c = 0.11\hbar/T_{c0}$. At $\tau < \tau_c$ the only phase which survives is the “weakly helical” state with $Q = 4\alpha H/v_F^2$; in this regime the paramagnetic critical field starts to *increase* with disorder, and at $\tau \ll \tau_c$ we find $H_c \propto \tau^{-1/2}$. In Sec. IX we go beyond the mean-field approximation and study the modifications of the transition line $T_c(H)$ due to the Berezinsky-Kosterlitz-Thouless vortex depairing transition. We demonstrate that vortex fluctuations are strongly enhanced near the points \mathcal{L} and \mathcal{S} , leading to local downward deformations of the actual $T_{BKT}(H)$ line.

II. MODEL OF A SPIN-ORBITAL SUPERCONDUCTOR

Near the surface of a crystal translational symmetry is reduced and inversion symmetry is broken even if it is present in the bulk. (The component of the electron momentum \hat{p} parallel to the interface is conserved because

of the remaining 2D translational symmetry.) As a result a transverse electrical field appears near the surface. The electron spin couples to this electric field due to the Rashba spin-orbit interaction⁷

$$H_{so} = \alpha \left[\hat{\sigma} \times \hat{p} \right] \cdot \vec{n}, \quad (1)$$

where $\alpha > 0$ is the spin-orbit coupling constant, \vec{n} is a unit vector perpendicular to the surface, $\hat{\sigma} = (\hat{\sigma}_x, \hat{\sigma}_y, \hat{\sigma}_z)$ are the Pauli matrices. This interaction explicitly violates inversion symmetry. The electron spin operator does not commute with the Rashba term, thus the spin projection is not a good quantum number. On the other hand, the chirality operator $[\hat{\sigma} \times \hat{e}] \cdot \vec{n}$ commutes with the Hamiltonian. Here $\hat{e} = \hat{p}/p$ is the momentum direction operator with eigenvalues $\vec{e}_{\mathbf{p}} = (\cos \varphi_{\mathbf{p}}, \sin \varphi_{\mathbf{p}})$, where $\varphi_{\mathbf{p}}$ is the angle between the momentum of the electron and the x -axis. The chirality operator eigenvalues $\lambda = \pm 1$ together with the momentum constitute the quantum numbers of the electron state (\vec{p}, λ) . The Rashba term (1) preserves the Kramers degeneracy of the electron states, thus the states (\vec{p}, λ) and $(-\vec{p}, \lambda)$ belong to the same energy.

In this paper we consider the simplest model³ of a surface superconductor: a BCS model for a two-dimensional metal with the Rashba term (1), in the limit $\alpha p_F \gg T_c$. The Hamiltonian written in the coordinate representation reads

$$\hat{H} = \int \psi_{\alpha}^{\dagger}(\vec{r}) \hat{h} \psi_{\beta}(\vec{r}) d^2\vec{r} - \frac{U}{2} \int \psi_{\alpha}^{\dagger} \psi_{\beta}^{\dagger} \psi_{\beta} \psi_{\alpha} d^2\vec{r}, \quad (2)$$

with the one-particle Hamiltonian operator

$$\hat{h} = \left(\frac{\hat{P}^2}{2m} \delta_{\alpha\beta} + \alpha \left[\hat{\sigma}_{\alpha\beta} \times \hat{P} \right] \cdot \vec{n} - g\mu_B \vec{h} \cdot \hat{\sigma}_{\alpha\beta}/2 \right), \quad (3)$$

where m is the electron mass, α, β are the spin indices and $\hat{P} = -i\vec{\nabla} - \frac{e}{c}\vec{A}(\vec{r})$ is the momentum operator in the presence of an infinitesimal in-plane vector potential $\vec{A} = \vec{A}(\vec{r})$, $e < 0$ is the electron charge. We have included into the Hamiltonian the Zeeman interaction with a uniform external magnetic field \vec{h} parallel to the interface, assuming \vec{h} to be in the x -direction. The vector potential of such a field can be chosen to have only the z -component, therefore it decouples from the 2D kinetic energy term. μ_B is the Bohr magneton and g is the Lande factor. Hereafter we use a notation $H = g\mu_B h/2$.

The electron operator can be expanded in the basis of plane waves: $\hat{\psi}_{\alpha}(\vec{r}) = \sum_{\mathbf{p}, \lambda} e^{i\mathbf{p}\vec{r}} a_{\alpha\mathbf{p}}$, and the one-particle part of the Hamiltonian (2) in the momentum representation can be written as a sum of \hat{H}_0 and \hat{H}_{em} :

$$\begin{aligned} \hat{H}_0 &= \sum_{\mathbf{p}} a_{\alpha\mathbf{p}}^{\dagger} \left(\frac{\mathbf{p}^2}{2m} \hat{1} + \alpha \left[\hat{\sigma}_{\alpha\beta} \times \mathbf{p} \right] \cdot \vec{n} - \vec{H} \cdot \hat{\sigma}_{\alpha\beta} \right) a_{\beta\mathbf{p}}, \\ \hat{H}_{em} &= \sum_{\mathbf{p}} a_{\alpha\mathbf{p}}^{\dagger} \left(-\frac{1}{c} \vec{j} \vec{A} \right) a_{\beta\mathbf{p}}. \end{aligned} \quad (4)$$

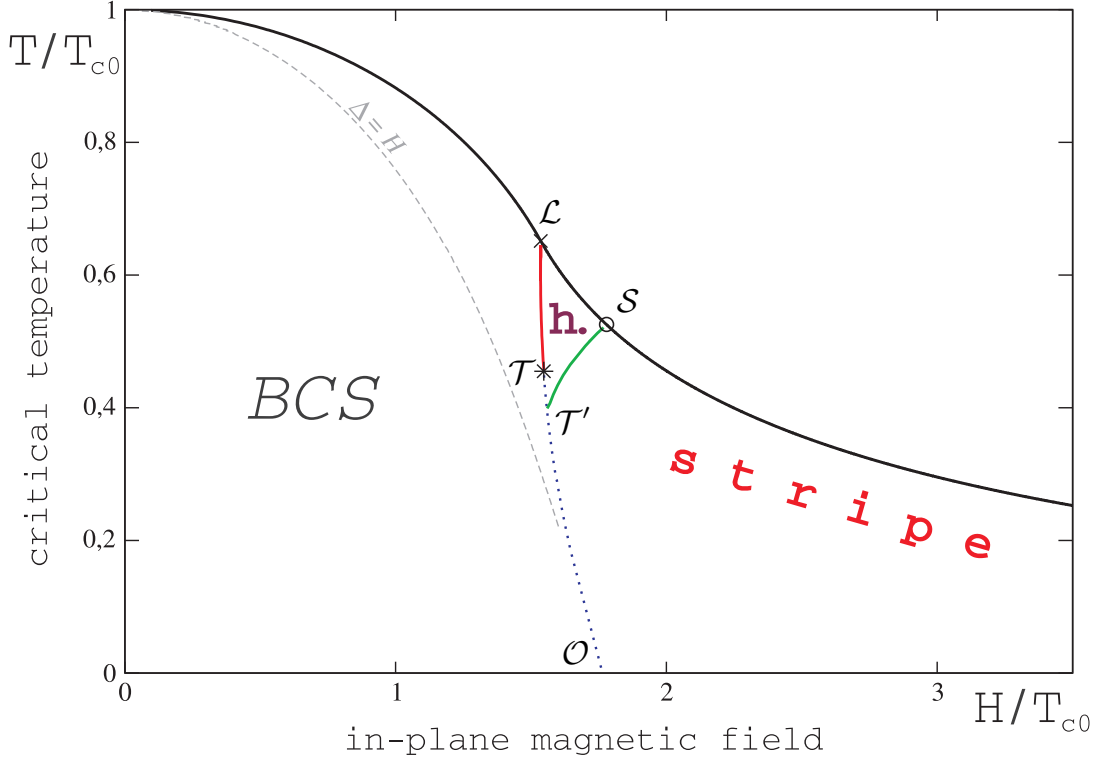


FIG. 1: A phase diagram that shows: a superconducting phase transition line $T_c(H)$ (solid) and two second-order phase transition lines in the clean case, an \mathcal{LT} line between the homogeneous (BCS) and the helical (h.) state, and an \mathcal{ST}' line of stability of the helical state. The dotted line going downwards from point \mathcal{T} to point \mathcal{O} marks the absolute limit of stability of the BCS state. The cross indicates the Lifshitz point \mathcal{L} and the circle indicates the symmetric point \mathcal{S} . The line of transition into the gapless superconductivity $H = \Delta$ is marked with a dashed line.

Here the current operator is

$$\hat{j} = -e(\hat{p}/m - \alpha[\hat{\sigma} \times \vec{n}]) - \frac{e^2}{2mc}\vec{A}. \quad (5)$$

The Hamiltonian \hat{H}_0 can be diagonalized by the transformation $a_{\alpha\mathbf{p}} = \eta_{\lambda\alpha}(\mathbf{p})\hat{a}_{\lambda\mathbf{p}}$ with the two-component spinor

$$\eta_{\lambda}(\mathbf{p}) = \frac{1}{\sqrt{2}} \begin{pmatrix} 1 \\ i\lambda \exp(i\varphi_{\mathbf{p}}(H)) \end{pmatrix}, \quad (6)$$

where

$$\varphi_{\mathbf{p}}(H) = \arcsin \frac{\alpha p_y - H}{\sqrt{(\alpha p)^2 - 2\alpha p_y H + H^2}}. \quad (7)$$

The eigenvalues of the Hamiltonian (4), corresponding to the chiralities $\lambda = \pm 1$, are

$$\epsilon_{\lambda}(\mathbf{p}) = p^2/2m - \lambda\sqrt{(\alpha p)^2 - 2\alpha p_y H + H^2}, \quad (8)$$

thus at $H = 0$ the equal-momentum electron states are split in energy by $2\alpha p_F$. The two Fermi circles, corresponding to the different chiralities, have Fermi-momenta $p_F^{\pm} = \sqrt{2m\mu + m^2\alpha^2 \pm m\alpha}$, where $\mu \gg m\alpha^2$ is the chemical potential. The density of states on the two Fermi circles is almost the same, $\nu_{\pm} = \frac{m}{2\pi} \left(1 \pm \frac{\alpha}{v_F}\right)$. In the main

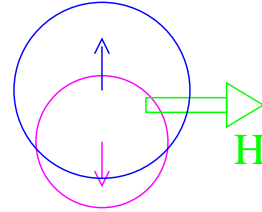


FIG. 2: When an external magnetic field $H \ll \alpha p_F$ is applied in the x -direction, the two Fermi circles corresponding to the different chiralities $\lambda = \pm 1$ are shifted in opposite y -directions by a small momentum $Q = \pm H/v_F$. The circle corresponding to one of the chiralities is larger than the other by the relative amount of α/v_F .

part of the paper we neglect the difference $\nu_+ - \nu_-$. The effects related to $\nu_+ \neq \nu_-$ will be considered in Sec. VII. When an external magnetic field is applied, these two Fermi circles are displaced in opposite y -directions by a momentum $Q = \pm H/v_F$, as shown in Fig. 2.

The two-particle pairing interaction in Hamiltonian (2) in the momentum representation reads

$$-\frac{U}{2} \sum_{\mathbf{p}\mathbf{p}'\mathbf{q}} a_{\alpha\mathbf{p}+\mathbf{q}/2}^+ a_{\beta-\mathbf{p}+\mathbf{q}/2}^+ a_{\beta-\mathbf{p}'+\mathbf{q}/2} a_{\alpha\mathbf{p}'+\mathbf{q}/2}, \quad (9)$$

and can be simplified in the chiral basis (6), assuming $H \ll \alpha p_F \ll \mu$. In the long-wavelength limit $q \ll p_F$ it can be factorized as

$$\hat{H}_{int} = -\frac{U}{4} \sum_{\mathbf{q}} \hat{A}^+(\mathbf{q}) \hat{A}(\mathbf{q}), \quad (10)$$

where the pair annihilation operator

$$\hat{A}(\mathbf{q}) = \sum_{\mathbf{p}, \lambda} \lambda e^{i\varphi_{\mathbf{p}}} a_{\lambda, -\mathbf{p}+\mathbf{q}/2} a_{\lambda, \mathbf{p}+\mathbf{q}/2}. \quad (11)$$

Here $\lambda e^{i\varphi_{\mathbf{p}}}$ is the wave function of the Cooper pair in the chiral basis and it changes sign under the substitution $-\mathbf{p}$ for \mathbf{p} .

To calculate the thermodynamic potential $\Omega = -T \ln Z$, we employ the imaginary-time functional integration technique with the Grassmanian electron fields $a_{\lambda\mathbf{p}}, \bar{a}_{\lambda\mathbf{p}}$ and introduce an auxiliary complex field $\Delta(\mathbf{r}, \tau)$ to decouple the pairing term H_{int} , cf. [11]. The resulting effective Lagrangian is

$$\begin{aligned} L[a, \bar{a}, \Delta, \Delta^*] = & \sum_{\mathbf{p}, \lambda} \bar{a}_{\lambda\mathbf{p}} (-\partial_{\tau} - \epsilon_{\lambda}(\mathbf{p})) a_{\lambda\mathbf{p}} + \\ & + \sum_{\mathbf{q}} \left[-\frac{|\Delta_{\mathbf{q}}|^2}{U} + \frac{1}{2} \sum_{\mathbf{p}, \lambda} (\Delta_{\mathbf{q}} \lambda e^{-i\varphi_{\mathbf{p}}} \bar{a}_{\lambda, \mathbf{p}+\mathbf{q}/2} \bar{a}_{\lambda, -\mathbf{p}+\mathbf{q}/2} \right. \\ & \left. + \Delta_{\mathbf{q}}^* \lambda e^{i\varphi_{\mathbf{p}}} a_{\lambda, -\mathbf{p}+\mathbf{q}/2} a_{\lambda, \mathbf{p}+\mathbf{q}/2} \right]. \end{aligned} \quad (12)$$

The thermodynamic potential $\Omega = -T \ln Z$ describes a system in equilibrium, where Z is the grand partition function. We express Ω as a zero-field limit of a generating functional $\Omega = \Omega[\eta, \bar{\eta}]|_{\eta \rightarrow 0}$:

$$\begin{aligned} \exp\left(-\frac{\Omega[\eta, \bar{\eta}]}{T}\right) &= \int \mathcal{D}\Delta \mathcal{D}\Delta^* \exp\left(-\frac{\Omega[\eta, \bar{\eta}, \Delta, \Delta^*]}{T}\right) = \\ &= \int \mathcal{D}a \mathcal{D}\bar{a} \mathcal{D}\Delta \mathcal{D}\Delta^* \exp\left(\int_0^{1/T} [L[a, \bar{a}, \Delta, \Delta^*] + \right. \\ &\quad \left. + \sum_{\mathbf{p}} (\bar{\eta}(\tau\mathbf{p}) a(\tau\mathbf{p}) + \bar{a}(\tau\mathbf{p}) \eta(\tau\mathbf{p}))] d\tau\right). \end{aligned} \quad (13)$$

Below we will work within the mean-field approximation, which is controlled by the smallness of the Ginzburg number Gi . However, for a clean 2D superconductor $Gi \sim T_c/E_F$ may be non-negligible (we discuss the fluctuational effects in the end of this paper). The mean-field approximation is equivalent to the saddle-point approximation for the functional integral over Δ and Δ^* defined in the first line in Eq. (13). In other terms, we will study the minima of the functional $\Omega[\Delta, \Delta^*]$, which comes about after integration over the Grassmanian fields in the functional integral defined in the second line of Eq. (13),

$$\frac{\delta\Omega[\Delta, \Delta^*]}{\delta\Delta(\tau\mathbf{r})} = 0. \quad (14)$$

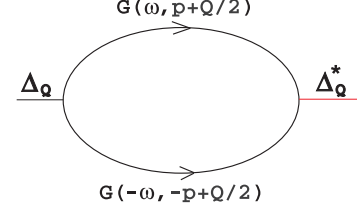


FIG. 3: A Cooper loop with transferred momentum Q .

To evaluate the thermodynamic potential $\Omega[\Delta, \Delta^*]$, we will use the Green's function method. The electron Green's function is defined as a variational derivative of the generating functional:

$$G(\tau\mathbf{r}, \tau'\mathbf{r}') = \frac{\delta\Omega[\eta, \bar{\eta}]}{\delta\bar{\eta}(\tau\mathbf{r})\delta\eta(\tau'\mathbf{r}')} \Big|_{\eta \rightarrow 0}. \quad (15)$$

In the next Section we determine the line of the superconducting transition $T_c(H)$, and locate two special points on this line, \mathcal{L} and \mathcal{T} , which designate the boundaries of different superconductive states.

III. SUPERCONDUCTING PHASE TRANSITION

Near the phase transition from a normal metal to a superconductor the order parameter $\Delta(\vec{r})$ is small. Therefore the thermodynamic potential Ω may be expanded in powers of $\Delta(\vec{r})$ and its gradients. This is known as the Ginzburg-Landau functional. It has been shown by Barzykin and Gor'kov⁴, that the ground state can be inhomogeneous in the direction perpendicular to the magnetic field. We consider the order parameter as a superposition of a finite number of harmonics:

$$\Delta(\vec{r}) = \sum_i \Delta_{\mathbf{Q}_i}(\vec{r}) \exp(i\mathbf{Q}_i \vec{r}), \quad (16)$$

where $\Delta_{\mathbf{Q}_i}(\vec{r})$ are slowly varying envelope functions. The corresponding Ginzburg-Landau functional is

$$\begin{aligned} \Omega_{sn} = & \int \left[\sum_i \alpha_{\mathbf{Q}_i \mathbf{Q}_i} |\Delta_{\mathbf{Q}_i}(\vec{r})|^2 + \right. \\ & + \sum_{ijkl} \beta_{\mathbf{Q}_i \mathbf{Q}_j \mathbf{Q}_k \mathbf{Q}_l} \Delta_{\mathbf{Q}_i}(\vec{r}) \Delta_{\mathbf{Q}_j}^*(\vec{r}) \Delta_{\mathbf{Q}_k}(\vec{r}) \Delta_{\mathbf{Q}_l}^*(\vec{r}) \times \\ & \quad \times \delta_{\mathbf{Q}_i + \mathbf{Q}_k - \mathbf{Q}_j - \mathbf{Q}_l} + \\ & + \sum_i c_{\mathbf{Q}_i \mathbf{Q}_i}^x \left| \left(-i\hbar \frac{\partial}{\partial x} - \frac{2e}{c} A_x(\vec{r}) \right) \Delta_{\mathbf{Q}_i}(\vec{r}) \right|^2 + \\ & \left. + \sum_i c_{\mathbf{Q}_i \mathbf{Q}_i}^y \left| \left(-i\hbar \frac{\partial}{\partial y} - \frac{2e}{c} A_y(\vec{r}) \right) \Delta_{\mathbf{Q}_i}(\vec{r}) \right|^2 \right] d^2\vec{r}. \end{aligned} \quad (17)$$

The coefficient $\alpha_{\mathbf{Q}\mathbf{Q}}$ is given by the Cooper loop diagram with transferred momentum Q . The coefficients

β_{QQQQ} and β_{QQ-Q-Q} are determined by four-Green's-function loop integrals:

$$\alpha_{QQ} = \frac{1}{U} - \frac{T}{2} \sum_{\omega, \mathbf{p}, \lambda} G_{\lambda}(\omega, \mathbf{p} + \mathbf{Q}/2) G_{\lambda}(-\omega, -\mathbf{p} + \mathbf{Q}/2), \quad (18)$$

$$\beta_{QQQQ} = T \sum_{\omega, \mathbf{p}, \lambda} G_{\lambda}^2(\omega, \mathbf{p} + \mathbf{Q}/2) G_{\lambda}^2(-\omega, -\mathbf{p} + \mathbf{Q}/2),$$

$$\begin{aligned} \beta_{QQ-Q-Q} &= T \sum_{\omega, \mathbf{p}, \lambda} G_{\lambda}^2(\omega, \mathbf{p} + \mathbf{Q}/2) \times \\ &\times G_{\lambda}(-\omega, -\mathbf{p} + \mathbf{Q}/2) G_{\lambda}(-\omega, -\mathbf{p} + 3\mathbf{Q}/2), \end{aligned} \quad (19)$$

$$c_{QQ}^{\mu} = \frac{1}{2} \frac{\partial^2}{\partial q_{\mu}^2} \alpha(Q \vec{e}_y + q_{\mu} \vec{e}_{\mu}). \quad (20)$$

Here the normal state Green's function in an external in-plane magnetic field $H \ll \alpha p_F$ is

$$G_{\lambda}(\omega, \mathbf{p}) = \frac{1}{i\omega - \xi_{\lambda}(\mathbf{p}) - \lambda H \sin \varphi_{\mathbf{p}}}, \quad (21)$$

where $\omega = 2\pi(n + \frac{1}{2})T$ is the Matsubara frequency, n is an integer, and the quasiparticle dispersion

$$\xi_{\lambda}(\mathbf{p}) = p^2/2m - \lambda \alpha p_F - \mu \quad (22)$$

is assumed to be small compared to αp_F . The integrals over the momenta in (18) and (19) are calculated in the semiclassical approximation:

$$\int \frac{d^2 \mathbf{p}}{(2\pi)^2} = \nu_{\lambda}(\epsilon_F) \int_{-\infty}^{\infty} d\xi_{\lambda} \int_0^{2\pi} \frac{d\varphi}{2\pi}. \quad (23)$$

In this Section we will calculate all diagrams in the zeroth order over the parameter $\alpha/v_F \ll 1$ (i. e. we approximate $\nu_{\lambda}(\epsilon_F) \approx \nu(\epsilon_F)$); the effect of the terms of the order of $O(\alpha/v_F)$ will be discussed in Sec. VII below.

Integrating over the momenta p in the Ginzburg-Landau functional coefficients gives

$$\alpha_{QQ} = \frac{1}{U} - \pi \nu(\epsilon_F) T \sum_{\omega > 0, \lambda} \frac{1}{\sqrt{\omega^2 + H_{\lambda}^2}}, \quad (24)$$

$$\beta_{QQQQ} = \frac{\nu(\epsilon_F)}{4} \pi T \sum_{\omega > 0, \lambda} \frac{2\omega^2 - H_{\lambda}^2}{(\omega^2 + H_{\lambda}^2)^{5/2}},$$

$$\beta_{QQ-Q-Q} = \frac{\nu(\epsilon_F)}{2} \pi T \sum_{\omega > 0, \lambda} \frac{(2\omega^2 + H_{\lambda}^2)}{\omega^2 (\omega^2 + H_{\lambda}^2)^{3/2}} \frac{H_{\lambda}}{v_F Q}, \quad (25)$$

$$c_{QQ}^x = c_{-Q-Q}^x = -\frac{1}{2} \left(\frac{v_F}{2} \right)^2 \pi \nu(\epsilon_F) T \sum_{\omega, \lambda} \frac{1}{(\omega^2 + H_{\lambda}^2)^{3/2}},$$

$$c_{QQ}^y = c_{-Q-Q}^y = -\frac{1}{2} \left(\frac{v_F}{2} \right)^2 \pi \nu(\epsilon_F) T \sum_{\omega, \lambda} \frac{2H_{\lambda}^2 - \omega^2}{(\omega^2 + H_{\lambda}^2)^{5/2}}, \quad (26)$$

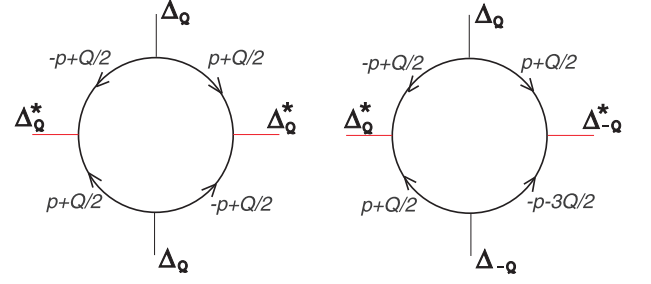


FIG. 4: Diagrams corresponding to the terms of the fourth order in Δ in the Ginzburg-Landau expansion: $\beta_{QQQQ}|\Delta_Q|^4$ and $\beta_{QQ-Q-Q}|\Delta_Q|^2|\Delta_{-Q}|^2$.

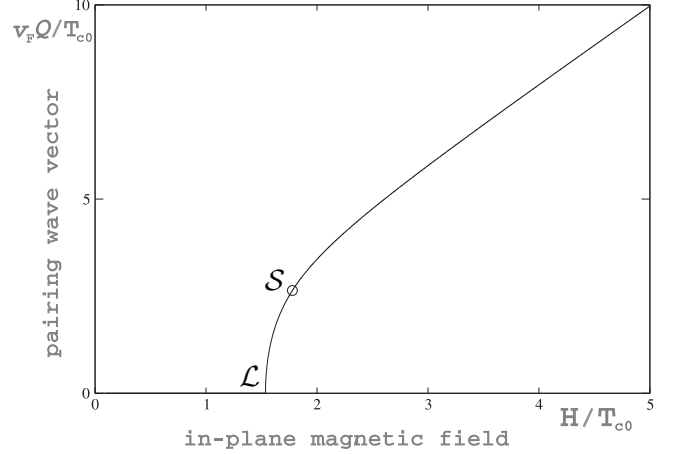


FIG. 5: Cooper pairing wave vector Q . The circle indicates the symmetric point S .

where

$$H_{\lambda} = \lambda H + v_F Q/2. \quad (27)$$

Note, that in the Ginzburg-Landau functional (17) the coefficients $\beta_{QQQQ} = \beta_{-Q-Q-Q-Q}$ correspond to the terms $|\Delta_Q|^4$ and $|\Delta_{-Q}|^4$; and the coefficient corresponding to the term $|\Delta_Q|^2|\Delta_{-Q}|^2$ is a sum of the four equal coefficients $\beta_{QQ-Q-Q} = \beta_{Q-Q-QQ} = \beta_{-Q-QQQ} = \beta_{-QQQ-Q}$.

The condition $\alpha_{QQ} = 0$ determines the second-order transition line (if $\beta_{QQQQ} > 0$) between the normal metal and the superconductor:

$$\frac{1}{U} = \nu(\epsilon_F) T \max_Q \sum_{\omega > 0, \lambda} \frac{\pi}{\sqrt{\omega^2 + (\lambda H + v_F Q/2)^2}}. \quad (28)$$

Equation (28) determines the shape of the phase transition line $T_c(H)$ between the normal and superconducting states. Depending upon H , the maximum over Q in the r.h.s. of Eq. (28) is attained either at $Q = 0$ or on nonzero $Q = \pm|Q|$. The position of the $T_c(H)$ line found via numerical solution of Eq. (28) is shown in Fig. 1, where both temperature T_c and in-plane magnetic field H are normalized by the critical temperature

at zero magnetic field: $T_{c0} = 2\omega_D \exp(-1/\nu U + \gamma)/\pi$, where $\gamma = 0.577$ is the Euler constant. The line $T_c(H)$ recovers two asymptotics found in [4]:

$$\log \frac{T_c(H)}{T_{c0}} = -\frac{7\zeta(3)H^2}{8\pi^2 T_{c0}^2} \quad \text{in the limit } H/T_{c0} \rightarrow 0,$$

$$\frac{T_c(H)}{T_{c0}} = \frac{\pi T_{c0}}{2e\gamma H} \quad \text{in the limit } H/T_{c0} \rightarrow \infty. \quad (29)$$

Whereas at low H the superconductive solution is uniform, $Q = 0$, in the high field limit one finds⁴ $Q = 2H/v_F$. The Lifshitz point \mathcal{L} separates $Q = 0$ and $Q \neq 0$ solutions on the $T_c(H)$ line and is the end of the second-order phase transition line between the two superconducting phases. In order to determine the position of the \mathcal{L} point, we note that α_{QQ} , cf. Eq. (24), is symmetric under the change $-Q \rightarrow Q$, and thus it has always an extremum at $Q = 0$. Therefore the position of the Lifshitz point \mathcal{L} should satisfy the equation

$$\left. \frac{\partial^2 \alpha_{QQ}}{\partial Q^2} \right|_{Q=0} = 0.$$

Numerical solution of the above equation gives the value $(H_L, T_L) = (1.536, 0.651)T_{c0}$, with the ratio $H_L/T_L \approx 2.36$.

Fig. 5 shows the Cooper pairing wave vector Q on the $T_c(H)$ line as a function of the in-plane magnetic field H . Near the \mathcal{L} point the wave-vector Q contains a square-root singularity $v_F Q(H) \sim \sqrt{H^2 - H_L^2}$, typical for the behavior of the order parameter near a second-order transition. In the high-field limit $H/T_c(0) \rightarrow \infty$ the behavior of the wave-vector Q is given by the asymptotic expression

$$v_F Q = 2H - \frac{\pi^4 T_c^4(0)}{7\zeta(3)e^2\gamma H^3}. \quad (30)$$

Note, that $Q = 2H/v_F$ is the momentum shift of the two $\lambda = \pm 1$ Fermi circles in a parallel magnetic field.

Near the $T_c(H)$ line the coefficient α can be approximated as

$$\alpha(T, H) \approx \nu(\epsilon_F) \frac{T - T_c(H)}{2T} \sum_{\lambda} Y(T_c(H), H_{\lambda}), \quad (31)$$

where $Y(T, \Delta) = 1 - T \sum_n \frac{\Delta^2 \pi}{(\omega_n^2 + \Delta^2)^{3/2}} = \frac{1}{4T} \int d\xi \operatorname{sech}^2 \frac{\sqrt{\xi^2 + \Delta^2}}{2T}$ is the Yosida function, $\omega_n = \pi T(2n + 1)$ is the Matsubara frequency. At $H > H_L$ an inhomogeneous superconductive phase is formed below the $T_c(H)$ line. Eq. (28) determines the absolute value of the equilibrium wave vector $|Q|$ (the direction of \mathbf{Q} is perpendicular to \mathbf{H}), therefore two harmonics may contribute to $\Delta(\vec{r})$ just below the $T_c(H)$ line: $\Delta(y) = \Delta_+ e^{iQy} + \Delta_- e^{-iQy}$. Below $T_c(H)$, the density of the thermodynamic potential Ω is lower in the superconductive state than in the normal one by the amount

$$\Omega_{sn} = \alpha(T, H)|\Delta|^2 + \beta_s(T, H)|\Delta|^4 + \beta_a(T, H)(|\Delta_+|^2 - |\Delta_-|^2)^2, \quad (32)$$

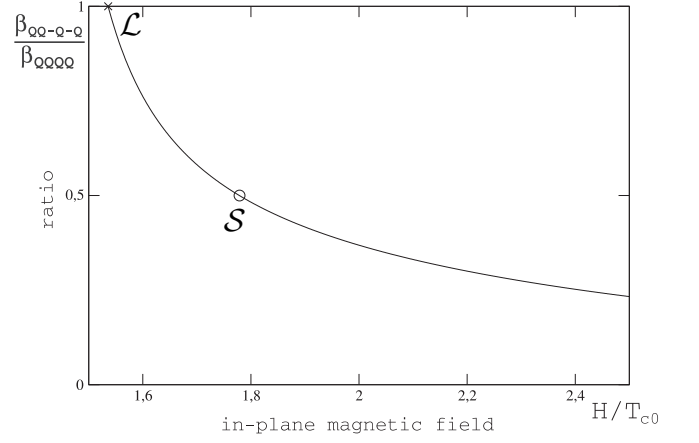


FIG. 6: The ratio of β_{QQ-Q-Q} and β_{QQQQ} coefficients. The symmetric point \mathcal{S} , marked on the figure with a circle, is defined as a point where the ratio attains the value $1/2$. The Lifshitz point \mathcal{L} is the point where the ratio equals 1, since $Q = 0$ there.

where $|\Delta|^2 = |\Delta_+|^2 + |\Delta_-|^2$. Eq. (32) was obtained from Eq. (17) by keeping of only two harmonics: $|\Delta_+|^2 = \Delta \mathbf{Q} \Delta^*$, $|\Delta_-|^2 = \Delta_- \mathbf{Q} \Delta_-^*$. Comparing Eqs. (17) and (32) gives

$$\beta_s(T, H) = \frac{1}{2} \beta_{QQQQ} + \beta_{QQ-Q-Q}, \quad (33)$$

$$\beta_a(T, H) = \frac{1}{2} \beta_{QQQQ} - \beta_{QQ-Q-Q},$$

where β_{QQQQ} and β_{QQ-Q-Q} are the four-Green's-function loop integrals (25). In the symmetric point \mathcal{S} , where $\beta_a(T_c(H), H) = 0$, the free energy (32) depends upon $|\Delta|^2$ only, and thus is invariant under $U(2)$ rotations of the order parameter spinor (Δ_+, Δ_-) . The coordinates of the \mathcal{S} point are: $(H_S, T_S) = (1.779, 0.525)T_{c0}$, the corresponding wave vector is $v_F Q_S = 2.647 T_{c0}$. At $H < H_S$ we find $\beta_a < 0$, and the free energy at $T < T_c(H)$ is minimized by the choice of either $\Delta_+ = 0$ or $\Delta_- = 0$, both corresponding to the helical state. At $H > H_S$ $\beta_a > 0$ and the free energy minimum is achieved at $|\Delta_+| = |\Delta_-|$, i. e. the LOFF-like phase with $\Delta(y) \propto \cos(Qy)$ is the stable one at high field values.

IV. UNUSUAL VORTEX SOLUTIONS NEAR THE SYMMETRIC POINT \mathcal{S} .

A. General considerations: extended $U(2)$ symmetry and vortices

In this Section we discuss the peculiar properties of the superconductive vortices, which appear due to the extended symmetry of the order parameter near the symmetric point \mathcal{S} of the phase diagram. The free energy of the superconductor in the vicinity of the symmetric point

is given by the Ginzburg-Landau functional

$$\begin{aligned} \Omega_{sn} = & \int d^2\vec{r} \left(c_i \left| \left(i\partial_i + \frac{2e}{c} A_i \right) \Delta_+ \right|^2 + \right. \\ & + c_i \left| \left(i\partial_i + \frac{2e}{c} A_i \right) \Delta_- \right|^2 + \beta_a (|\Delta_+|^2 - |\Delta_-|^2)^2 + \\ & \left. + \beta_s (\Delta_0^2 - |\Delta_+|^2 - |\Delta_-|^2)^2 - \beta_s \Delta_0^4 \right), \end{aligned} \quad (34)$$

where $i = x, y$, and $\Delta_0^2 = -\alpha/2\beta_s$ is the equilibrium value of the order parameter. The fourth-order term in the Ginzburg-Landau expansion (32) can be divided into a symmetric and an anisotropy part $\beta_a(T, H)(|\Delta_+|^2 - |\Delta_-|^2)^2$, and in the symmetric point the coefficient $\beta_a(T_S, H_S) = 0$. The coefficients c_x, c_y are given by the expressions (26), and their ratio in the \mathcal{S} point is equal to $c_x/c_y = 1.72$. Eq. (34) can be written in a rotationally symmetric form via an area-conserving transformation by stretching and contracting the two coordinates $x \rightarrow x(c_x/c_y)^{1/4}$ and $y \rightarrow y(c_y/c_x)^{1/4}$.

The minimum of the free energy (34) in the symmetric point (where $\beta_a = 0$) is achieved in the homogeneous state under the condition $|\Delta_+|^2 + |\Delta_-|^2 = \Delta^2$. In normalized variables $z_1 = \Delta_+/\Delta$ and $z_2 = \Delta_-/\Delta$ the order parameter spinor (z_1, z_2) spans the sphere S^3 : $|z_1|^2 + |z_2|^2 = 1$, and is equivalent to a four-component unit vector \vec{N} . This normalization allows us to write the gradient part of the free energy (34) as a non-linear sigma-model

$$F_{\text{grad}} = \frac{\rho_s}{2} \int d^2\vec{r} (\partial_\mu \vec{N})^2, \quad (35)$$

where $\rho_s = \frac{|\alpha|}{\beta_s} \sqrt{c_x c_y}$ is defined through coefficients of the Ginzburg-Landau functional (34).

Precisely at the symmetric point, the gradient functional (35) governs the system's behavior at length scales L larger than the order parameter correlation length $\xi(T)$. At $\beta_a \neq 0$ its applicability is limited from the large scales also. Namely, L should be smaller than the temperature-dependent “anisotropy length”

$$L_{\text{an}}(T) = \xi(T) \sqrt{\frac{\beta_s}{|\beta_a|}} \gg \xi(T), \quad (36)$$

which is determined by comparison of the gradient term and the anisotropy term in the full free energy functional (34).

On the left of the symmetric point ($\beta_a < 0$) the minimum of the energy is achieved at either $|z_1| = 1$ or $|z_2| = 1$, leading to the degeneracy manifold of the order parameter, $S^1 \otimes Z_2$. On the right of the symmetric point ($\beta_a > 0$) the degeneracy manifold of the order parameter is $S^1 \otimes S^1$. In order for the gradient energy of a physical defect to be finite, at large distances from the defect core the order parameter should belong to the corresponding degeneracy manifold. On the other hand, at relatively

small distances $r \leq L_{\text{an}}$, the whole S^3 sphere is available for the order parameter configurations.

The two-dimensional x -space is topologically equivalent to a sphere S^2 with a boundary at infinity S^1 . A physical defect is described as a mapping of a disk on the real plane R^2 with a boundary S^1 (which encloses the defect) on the degeneracy manifold of the order parameter S^3 . Due to boundary conditions at infinity (imposed by the anisotropy) the mapping $S^2 \rightarrow S^3$ is accompanied either by the mapping $S^1 \rightarrow S^1$ (at $\beta_a < 0$, i. e. on the left from the \mathcal{S} point), or by $S^1 \rightarrow S^1 \otimes S^1$ (at $\beta_a > 0$). Therefore the topological defects are determined by the nontrivial elements of the homotopy group $\pi_2(S^3, S^1) = Z$ (on the left from the \mathcal{S} point) or $\pi_2(S^3, S^1 \otimes S^1) = Z \otimes Z$ (on the right from the \mathcal{S} point). Note that in the absence of any anisotropy there would be no stable topological defects since $\pi_2(S^3) = 0$, i. e. any configuration of the order parameter could be transformed into a homogeneous state. The general approach to the classification of vortices with a nonsingular core by means of the relative homotopy groups $\pi_2(R, \vec{R})$, described above, was first introduced by Minneev and Volovik [12]; a review of the approach can be found in [13]. Some explicit solutions for nonsingular vortices are presented in the review [14].

For an actual calculation it is convenient to employ the Hopf projection, which splits the order parameter spinor $z \in S^3$, parameterized here as

$$z = \begin{pmatrix} z_1 \\ z_2 \end{pmatrix} = e^{i\chi} \begin{pmatrix} e^{-i\varphi/2} \cos \theta/2 \\ e^{i\varphi/2} \sin \theta/2 \end{pmatrix}, \quad (37)$$

into an $N = 3$ - unit vector $\vec{n} = z^\dagger \vec{\sigma} z \in S^2$ sphere,

$$\vec{n} = \begin{pmatrix} \sin \theta \cos \varphi \\ \sin \theta \sin \varphi \\ \cos \theta \end{pmatrix}, \quad (38)$$

parameterized through the Euler angles on the S^2 sphere, and a total phase $\chi \in U(1)$, canonically conjugated to the electron charge.

Each configuration $\vec{n}(x)$ defines a mapping of the coordinate plane (equivalent to S^2) on a sphere $\vec{n}^2 = 1$, i. e. the mapping $S^2 \rightarrow S^2$. These mappings are characterized by an integer “topological charge”

$$\mathcal{Q} = \frac{1}{4\pi} \int_{R^2} \vec{n} [\partial_x \vec{n} \times \partial_y \vec{n}] d^2\vec{r}, \quad (39)$$

which is related with the circulation of the vector

$$\mathcal{A}_\mu = -i(z^\dagger \partial_\mu z - z \partial_\mu z^\dagger) = (\partial_\mu \chi - \frac{1}{2} \partial_\mu \varphi \cos \theta). \quad (40)$$

Indeed the following identity can be proven:

$$\mathcal{Q} = \frac{1}{2\pi} \oint_{C_\infty} \vec{\mathcal{A}} \cdot d\vec{l} - \frac{1}{2\pi} \oint_{C_0} \vec{\mathcal{A}} \cdot d\vec{l} \equiv \frac{\Phi}{\Phi_0} - C_0, \quad (41)$$

where C_∞ is the closed loop at infinity, and C_0 is the infinitesimal closed loop just around the vortex singularity point. The last equality in Eq. (41) relates the topological charge \mathcal{Q} and the magnetic flux connected with the vortex defect (in units of the superconductive flux quantum Φ_0).

Now the gradient energy (35) can be represented as a sum of the gradient energy of the \vec{n} -field and the kinetic term:

$$F_{\text{grad}} = \frac{\rho_s}{2} \int \left[\frac{1}{4} (\partial_\mu \vec{n})^2 + \mathcal{A}_\mu^2 \right] d^2 \vec{r}. \quad (42)$$

Below we consider separately vortex solutions in the helical state realized at $\beta_a < 0$ and in the LOFF-like state at $\beta_a > 0$.

B. Non-singular vortices in the helical state.

In the region on the left of the symmetric point ($\beta_a < 0$) the energy minimum in the bulk of the film is attained at either $z_1 = 1$, $z_2 = 0$ or vice versa; we choose the first solution for further discussions. Then the order parameter is proportional to $e^{i(\chi - \varphi/2)}$ and an elementary vortex corresponds to the rotation by 2π of the “effective” parameter’s phase $\chi - \varphi/2 = \phi$, where ϕ is the azimuthal angle on the plane. Near the vortex core, however, one can construct solutions which contain both z_1 and z_2 components. Now we show that such a solution has a lower energy than that of a standard singular vortex (like those in He-II or strongly type-II superconductors).

Indeed, one can employ a vortex trial solution

$$z_1 = \frac{re^{i\phi}}{\sqrt{R^2 + r^2}}, \quad z_2 = \frac{R}{\sqrt{R^2 + r^2}}, \quad (43)$$

which satisfies the boundary conditions : only one component $z_1 = \frac{\Delta_+}{|\Delta|} = e^{i\phi}$ survives on large distances. The solution (43) possesses a topological charge $\mathcal{Q} = 1$, and it is just the skyrmion [15, 16] for the $N = 3$ non-linear sigma model functional (i. e. the first term in the free energy (42))

$$E_{\text{Skyrm}} = \frac{\rho_s}{2} \int \frac{1}{4} (\partial_\mu \vec{n})^2 d^2 \vec{r}. \quad (44)$$

Note, however, that here we use a different gauge. The solution (43) corresponds to choice of the phases

$$\chi = -\varphi/2 = \phi/2. \quad (45)$$

The parameter R is an arbitrary number: at any R the topological charge of the skyrmion is $\mathcal{Q} = 1$ and its energy

$$E_{\text{Skyrm}} = \pi \rho_s.$$

However, the full gradient functional (42) contains the second term as well. This term leads to logarithmically

large energy

$$E_2 = \pi \rho_s \log \frac{\Lambda}{R}, \quad (46)$$

where Λ is the minimal of the system size and (a very long) two-dimensional screening length $\lambda_{2D} = 2\lambda^2/d$. Indeed, at $r \geq R$ one finds $\mathcal{A}_\mu^2 = r^{-2}$, whereas at $r \ll R$ the polar angle $\theta \rightarrow \pi$ and, according to Eqs. (40, 45) the “vector potential” \mathcal{A}_μ is not singular anymore. It is evident from Eq. (46) that one should choose R as large as possible in order to minimize vortex energy. The upper limit is given by the anisotropy length L_{an} defined in Eq. (36). Thus the minimal energy of our trial solution can be estimated as

$$E_{\text{cont}} = \pi \rho_s (\log \Lambda/L_{\text{an}} + C), \quad (47)$$

where $C \sim 1$. The energy of the continuous vortex (47) is lower than the energy of a usual singular vortex by a large amount

$$E_{\text{sing}} - E_{\text{cont}} = \frac{\pi}{2} \rho_s \log \frac{\beta_s}{|\beta_a|}. \quad (48)$$

We emphasize, that the solution (43) does not provide the energy minimum but is just a trial function; the correct non-singular vortex solution should have even lower energy and thus is more stable than the singular vortex. In the case of a continuous vortex the term C_0 in Eq. (41) is zero and $\mathcal{Q} = \Phi/\Phi_0$, whereas for a singular vortex $C_0 = \pm 1$ and $\mathcal{Q} = 0$.

C. Half-quantum vortices in the LOFF state

The LOFF-like (or “stripe”) state is realized at $\beta_a > 0$ and its degeneracy manifold is $S^1 \otimes S^1$. Indeed, the energy minimum is realized when vector \vec{n} is parameterized as $\vec{n} = (\cos \varphi, \sin \varphi, 0)$, i. e. $\theta = \pi/2$, thus there are two phase variables, φ and χ , cf. parameterization (37, 38). A usual singular vortex solution corresponds to $\varphi = \text{const}$ and $\delta\chi = 2\pi$; according to Eq. (40), in this case the “vector potential” $\mathcal{A}_\mu = \partial_\mu \chi$, and it does not contain the second phase φ . Then a natural question arises, if some other vortex-like solutions are possible, due to the extended (with respect to the usual S^1) degeneracy manifold. Indeed, the same degeneracy manifold of the order parameter is realized in some of the p-wave superconductive states, leading to the existence of half-quantum vortices^{17,18,19}. The reason for the existence of such an object is evident from the representation (37): a sign-change of the order parameter due to the π -rotation of the phase χ along some closed loop in real space can be compensated by the $\pm 2\pi$ -rotation of the phase φ along (topologically) the same loop.

We are not aware of any explicit solution for a half-vortex in the general case of an $S^1 \otimes S^1$ degeneracy manifold. However, some progress can be made in the vicinity

of the symmetric point \mathcal{S} , where $\beta_a \ll \beta_s$ and the problem simplifies a bit due to the presence of the “isotropic” spatial scales, $\xi(T) \ll L \ll L_{\text{an}}(T)$, cf. Eq. (36). Indeed, on such length-scales the problem can be treated within the gradient free energy, cf. Eq. (35) or Eq. (42). The solutions with half-quantum of magnetic flux obey boundary conditions $\theta(\infty) = \pi/2$ and $\delta_\infty \varphi = \pm 2\pi$, where via δ_∞ we denoted the phase increment along the large loop. Explicit form of these solutions may be ($\tilde{z}_i = \sqrt{2}z_i$)

$$\begin{aligned} \tilde{z}_1 &= \sqrt{1 - \frac{R}{\sqrt{r^2 + R^2}}} e^{i\gamma\phi}, & \tilde{z}_2 &= \sqrt{1 + \frac{R}{\sqrt{r^2 + R^2}}} \\ & & & \text{and} \\ \tilde{z}_1 &= \sqrt{1 + \frac{R}{\sqrt{r^2 + R^2}}}, & \tilde{z}_2 &= \sqrt{1 - \frac{R}{\sqrt{r^2 + R^2}}} e^{i\gamma\phi}, \end{aligned} \quad (49)$$

with an arbitrary parameter R . The variable $\gamma = \pm 1$ in the exponent of Eq. (49) corresponds to the sign of the vorticity (the magnetic flux), whereas the first and the second lines in Eq. (49) correspond to the cases of negative and positive projections n_3 of the \vec{n} vector in the center of the half-vortex. In terms of vector \vec{n} these four solutions (49) are represented as follows:

$$\vec{n}_{1,2} = \frac{1}{\sqrt{r^2 + R^2}} \begin{pmatrix} x \\ -\gamma y \\ -R \end{pmatrix}, \quad \vec{n}_{3,4} = \frac{1}{\sqrt{r^2 + R^2}} \begin{pmatrix} x \\ \gamma y \\ R \end{pmatrix}. \quad (50)$$

An elementary calculation of the topological charge and of the magnetic flux associated with the vortex solution Eq. (50) leads to

$$\mathcal{Q} = \frac{\Phi}{\Phi_0} = \frac{\gamma}{2}. \quad (51)$$

An additional binary variable which characterizes the half-vortex is the sign of the component $n_3(r=0)$. Therefore, totally there are 4 types of half-quantum vortices.

In the presence of a finite length L_{an} the solutions (49) make sense as intermediate asymptotics, as long as $R \ll L_{\text{an}}$, whereas at longer scales the anisotropic term $\propto \beta_a$ modifies the solution considerably (a numerical solution would be necessary to determine the solution in this region). Nevertheless, we can make an energy comparison between the singular vortex and a pair of half-quantum vortices even without an explicit solution including the anisotropic term. Consider two contributions to the free energy functional (42). The term with $\partial_\mu \vec{n}$, evaluated for the solution (50), gives (the main contribution comes from large distances, $r \gg R$)

$$E_{\vec{n}} \approx \frac{\pi}{4} \rho_s \log \frac{\Lambda}{R},$$

whereas the term with \mathcal{A}_μ contributes with about the same amount (since \mathcal{A}_μ is non-singular at small $r \leq R$)

$$E_{\mathcal{A}} \approx \frac{\pi}{4} \rho_s \log \frac{\Lambda}{R}.$$

Both above estimates may contain subleading terms $\sim \rho_s$ which we do not control. Totally, the energy of a half-vortex is

$$E_{1/2} = \frac{\pi}{2} \rho_s \left(\log \frac{\Lambda}{R} + C_{1/2} \right), \quad (52)$$

where $C_{1/2} \sim 1$. The minimal energy of a half-vortex can be estimated from Eq. (52) with the substitution $R \sim L_{\text{an}}$. Thus we find that the energy of two half-vortices coincides (up to the terms $\sim \rho_s$ which do not contain a large logarithm) with the energy of a continuous single-quantum vortex (47), found in the previous Subsection, and is certainly lower than the energy of the singular vortex by approximately the same amount as in Eq. (48). This means that the half-quantum vortex is a fundamental topological defect of the stripe (LOFF) state, at least in the region relatively close to the symmetric point \mathcal{S} .

V. PHASE DIAGRAM

A. Stationary conditions for the helical phase

Now we concentrate on the properties of the helical phase significantly below $T_c(H)$, and determine the locations of the phase transition lines \mathcal{LT} , \mathcal{ST}' and \mathcal{TO} . This calculation is possible since $|\Delta(\vec{r})|^2 = \text{const}$ in the helical state, and thus explicit analytic equations determining Δ and the corresponding Q can be written without resorting to an expansion over small Δ . Evaluation of the thermodynamic potential in the helical state gives

$$\begin{aligned} \Omega_{\text{hel}}(\Delta, H) &= \frac{\Delta^2}{U} - \\ &\pi \nu(\epsilon_F) T \sum_{\omega, \lambda} \int_0^{2\pi} \left(\sqrt{\tilde{\omega}^2 + \Delta^2} - |\tilde{\omega}| \right) \frac{d\varphi}{2\pi}, \end{aligned} \quad (53)$$

where

$$\tilde{\omega} = \omega + iH_\lambda \sin \varphi, \quad (54)$$

and H_λ is determined in Eq. (27). The equations determining Δ and Q are derived from the two stationary conditions

$$\frac{\partial \Omega_{\text{hel}}}{\partial \Delta} = \frac{2\Delta}{U} - \pi \nu(\epsilon_F) T \sum_{\omega, \lambda} \int_0^{2\pi} \frac{\Delta}{\sqrt{\tilde{\omega}^2 + \Delta^2}} \frac{d\varphi}{2\pi} = 0 \quad (55)$$

and

$$\frac{\partial \Omega_{\text{hel}}}{\partial Q} = \frac{v_F}{2} \nu(\epsilon_F) T \sum_{\omega, \lambda} f(H_\lambda, \omega) = 0, \quad (56)$$

where we denoted $f(H_\lambda, \omega) = -i \int_0^{2\pi} \frac{\tilde{\omega} \sin \varphi}{\sqrt{\tilde{\omega}^2 + \Delta^2}} \frac{d\varphi}{2}$.

Reducing the integrals over φ in Eqs. (55, 56) to complete elliptic integrals (see Appendix 1) compacts the

stationary conditions to a two equations set

$$\frac{1}{U} = 2\nu(\epsilon_F)T \sum_{\omega>0,\lambda} \frac{\mathbf{K}(k)}{\sqrt{\omega^2 + (|H_\lambda| + \Delta)^2}}, \quad (57)$$

$$\sum_{\omega>0,\lambda} f(H_\lambda, \omega) = 0, \quad (58)$$

where the Jacobi modulus

$$k = \frac{2\sqrt{\Delta|H_\lambda|}}{\sqrt{\omega^2 + (|H_\lambda| + \Delta)^2}}, \quad (59)$$

and the function

$$f(H_\lambda, \omega) = \frac{1}{H_\lambda} \left((\omega^2 + H_\lambda^2 + \Delta^2) \frac{\mathbf{K}(k)}{\sqrt{\omega^2 + (|H_\lambda| + \Delta)^2}} - \sqrt{\omega^2 + (|H_\lambda| + \Delta)^2} \mathbf{E}(k) \right) \quad (60)$$

is defined through the Jacobi complete elliptic integrals of the first and second kind. At $\Delta = 0$ Eq. (57) reduces to Eq. (28).

B. Lifshitz phase transition line \mathcal{LT}

The thermodynamic potential (53) in the helical state is a function of Q for any given pair (H, T) by virtue of Eqs. (57, 58). At small Q Eq. (53) can be expanded in powers of Q as (terms of the order of α/v_F have been neglected)

$$\Omega_{hel}(Q) = \Omega_{hel}(0) + aQ^2 + bQ^4 + cQ^6, \quad (61)$$

where

$$a = \frac{1}{2} \frac{\partial^2 \Omega}{\partial Q^2} = \left(\frac{v_F}{2} \right)^2 \nu(\epsilon_F)T \sum_{\omega,\lambda} \int_0^{2\pi} \frac{\Delta^2 \sin^2 \varphi}{(\tilde{\omega}^2 + \Delta^2)^{3/2}} \frac{d\varphi}{2}, \quad (62)$$

$$24b = \frac{d^4 E}{dQ^4} = \frac{\partial^4 \Omega}{\partial Q^4} - 3 \frac{\left(\frac{\partial^3 \Omega}{\partial \Delta \partial Q^2} \right)^2}{\frac{\partial^2 \Omega}{\partial \Delta^2}} \quad (63)$$

and $c > 0$. The condition $a = 0$, $b > 0$ determines the second-order Lifshitz phase transition line \mathcal{LT} , which ends at the critical point \mathcal{T} , where the coefficient $b = 0$ changes sign, see Fig. 1. The condition $a = 0$ may be simplified after reducing the integrals over φ in Eq. (62):

$$\sum_{\omega>0} \left(J + 2\omega \frac{\partial}{\partial \omega} J + \frac{\Delta^2 - \omega^2}{\Delta} \frac{\partial}{\partial \Delta} J \right) = 0, \quad (64)$$

where

$$J = \frac{\mathbf{K} \left(\sqrt{\frac{4\Delta H}{\omega^2 + (H + \Delta)^2}} \right)}{\sqrt{\omega^2 + (H + \Delta)^2}}.$$

The line \mathcal{LO} of stability of the BCS state (with respect to a formation of the helical wave) is determined by a simultaneous numerical solution of Eqs. (57, 58), taken at $Q = 0$, and Eq. (64). This line is indeed a line of a second-order transition as long as the coefficient $b > 0$. Using Eqs. (53, 58), we compute the coordinates of the point $\mathcal{T} \in \mathcal{LO}$ where $b = 0$ (cf. Eq. (63) for b) as $(H, T) = (1.547, 0.455)T_{c0}$. At lower temperatures $b < 0$ and a first-order transition out of the homogeneous state takes place. Therefore \mathcal{TO} is a boundary of a domain of the BCS state local stability. The actual first-order transition line \mathcal{TO}' between the BCS and some inhomogeneous state consisting of many spatial harmonics lays at lower values of the magnetic field ($H_{O'} < H_O = 1.76T_{c0}$).

The homogeneous superconductor which exists on the left of the Lifshitz line is “gapless” for high enough temperatures. The spectrum of the particles is $E_{\mathbf{p}} = \sqrt{\xi^2 + \Delta^2} - \lambda H \sin \varphi_{\mathbf{p}}$, therefore the minimum bound energy of the Cooper pairs (the energy gap) turns to zero at $H \geq \Delta$. The line of transition into the gapless superconductivity $H = \Delta$ is marked in Fig. 1 with a dashed line.

C. Phase transition line \mathcal{ST}'

The second-order phase transition line \mathcal{ST}' bounds the region of the helical phase from the high- H side. Its position can be determined via the stability condition with respect to the additional modulations of the order parameter, of the form $\delta\Delta(\vec{r}) = \delta v_{-q} \exp(-iqy) + \delta v_{q+2Q} \exp(i(q+2Q)y)$:

$$\delta\Omega_{\delta v} = \vec{v}^+ \hat{\mathcal{A}}(q) \vec{v}, \quad (65)$$

where $\vec{v} = (\delta v_{-q}, \delta v_{q+2Q}^*)$ and

$$\hat{\mathcal{A}}(q) = \frac{1}{U} - \sum_{\omega>0, \mathbf{p}, \lambda} \begin{pmatrix} G_{\lambda p_-} G_{\lambda -p_+} & F_{\lambda p_-} F_{\lambda -p_+} \\ F_{\lambda p_-}^* F_{\lambda -p_+}^* & G_{\lambda p_+ + Q} G_{\lambda -p_- + Q} \end{pmatrix}, \quad (66)$$

whith $p_{\pm} = p \pm q/2$. The Green's functions entering the matrix $\hat{\mathcal{A}}$ are

$$\begin{aligned} G_{\lambda} \left(\omega, \mathbf{p} - \frac{\mathbf{q}}{2} \right) &= -\frac{i\tilde{\omega} + \xi - Q_{\mathbf{p}}}{\tilde{\omega}^2 + (\xi - Q_{\mathbf{p}})^2 + \Delta^2}, \\ F_{\lambda} \left(\omega, \mathbf{p} - \frac{\mathbf{q}}{2} \right) &= \frac{\lambda e^{-i\varphi_{\mathbf{p}}} \Delta}{\tilde{\omega}^2 + (\xi - Q_{\mathbf{p}})^2 + \Delta^2} = \\ &= -F_{\lambda} \left(-\omega, -\mathbf{p} + \frac{\mathbf{q}}{2} + \mathbf{Q} \right), \end{aligned} \quad (67)$$

where $\tilde{\omega}$ is given by (54), and for brevity we introduced a notation $Q_{\mathbf{p}} = (q + Q) \sin \varphi_{\mathbf{p}}/2$.

The matrix $\hat{\mathcal{A}}$ has two eigenvalues $\epsilon_1(q) < \epsilon_2(q)$,

$$\begin{aligned} \epsilon_{2,1}(q) &= \\ &= \left(\frac{1}{U} - \frac{g_{-q} + g_{q+2Q}}{2} \right) \pm \sqrt{\left(\frac{g_{-q} - g_{q+2Q}}{2} \right)^2 + |f_{-q}|^2}, \end{aligned}$$

where

$$\begin{aligned} \frac{1}{U} - \frac{g_{-q} + g_{q+2Q}}{2} &= \\ &= \sum_{\omega > 0, \lambda} \int_0^{2\pi} \frac{d\varphi}{4} \frac{1}{\sqrt{\tilde{\omega}^2 + \Delta^2}} \left(1 - \frac{\tilde{\omega}^2 - Q_{\mathbf{p}}^2}{\tilde{\omega}^2 + Q_{\mathbf{p}}^2 + \Delta^2} \right), \\ \frac{g_{-q} - g_{q+2Q}}{2} &= \sum_{\omega > 0, \lambda} \int_0^{2\pi} \frac{d\varphi}{4} \frac{1}{\sqrt{\tilde{\omega}^2 + \Delta^2}} \frac{2i\tilde{\omega}Q_{\mathbf{p}}}{\tilde{\omega}^2 + Q_{\mathbf{p}}^2 + \Delta^2}, \\ f_{-q} &= \sum_{\omega > 0, \lambda} \int_0^{2\pi} \frac{d\varphi}{4} \frac{1}{\sqrt{\tilde{\omega}^2 + \Delta^2}} \frac{\Delta^2}{\tilde{\omega}^2 + Q_{\mathbf{p}}^2 + \Delta^2}. \end{aligned} \quad (68)$$

Here $g_{-q} = \sum_{\omega > 0, \mathbf{p}, \lambda} G_{\lambda, \mathbf{p}-\mathbf{q}/2} G_{\lambda, -\mathbf{p}-\mathbf{q}/2}$, $g_{q+2Q} = \sum_{\omega > 0, \mathbf{p}, \lambda} G_{\lambda, \mathbf{p}+\mathbf{q}/2+\mathbf{Q}} G_{\lambda, -\mathbf{p}+\mathbf{q}/2+\mathbf{Q}}$ and $f_{-q} = \sum_{\omega > 0, \mathbf{p}, \lambda} F_{\lambda, \mathbf{p}-\mathbf{q}/2} F_{\lambda, -\mathbf{p}-\mathbf{q}/2}$. The integrals (68) can be expressed through the elliptic integrals of the first and the second kind, as shown in Appendix 2.

The helical state metastability line \mathcal{ST}' is defined as a set of points where one mode δv becomes energetically favorable: $\min_q \epsilon_1(q) = 0$. Four equations are to be solved simultaneously in order to find the position of this line: two gap equations (57, 58), that determine the equilibrium Δ and Q , together with the two equations $\partial_q \epsilon_1(q) = 0$ and $\epsilon_1(q) = 0$, where $\epsilon_1(q)$ is determined in (68). We call the new phase on the right of the \mathcal{ST}' transition line a “three-exponential” state.

Note, that the \mathcal{ST}' line is an actual phase transition line out of the helical state *if* this transition is of the second order. Another possibility might be that a first-order transition occurs, which transforms the helical state into parity-even LOFF-type state, and occurs at slightly lower values of H at each T . Below we show that near $T_c(H)$ the phase transition is indeed of the second order. In order to demonstrate it, we evaluate terms of the eighth order in $|\Delta_Q|$ in the Ginzburg-Landau functional. Parameterizing the order parameter spinor near the symmetric point as

$$\begin{pmatrix} \Delta_+ \\ \Delta_- \end{pmatrix} = \Delta e^{i\chi} \begin{pmatrix} e^{-i\varphi/2} \cos \theta/2 \\ e^{i\varphi/2} \sin \theta/2 \end{pmatrix}, \quad (69)$$

the anisotropy part in the Ginzburg-Landau functional reads

$$\Omega_{sn}^{anis}(\kappa) = \beta_a \Delta^4 \cos^2 \theta + \kappa \Delta^8 \cos^4 \theta \quad (70)$$

(note that the term $\propto |\Delta|^6$ is not allowed by symmetry). The sign of the coefficient κ in front of the term $\cos^4 \theta$ determines the type of the transition near the $T_c(H)$ line. We demonstrate, by rather tedious calculations described in Appendix 3, that $\kappa > 0$, which proves that the transition is of the second order near the $T_c(H)$ line.

Now we come to somewhat surprising situation. Indeed, according to the analysis of superconductive instability at the $T_c(H)$ line, on the right of the symmetric point \mathcal{S} the stripe (LOFF-like) state is formed, which contains two harmonics with $Q = \pm|Q|$. Such a

phase preserves spatial inversion (in the plane) and time-reversal symmetry. Below the $T_c(H)$ line additional harmonics develop in such a phase, but they come in pairs $\pm 3Q, \pm 5Q, \dots$, and still preserve spatial and time-reversal symmetry. On the other hand, the second-order phase transition line \mathcal{ST}' separates the helical state (parity-odd) and a “three-exponential” state which has broken parity and time-reversal symmetry as well. It means that there must exist one more phase transition line, between the “three-exponential” phase and the parity-even stripe phase. This transition line should start at point \mathcal{S} but will lie slightly to the right from the line \mathcal{ST}' , i. e. at higher values of the field.

The fact that the points \mathcal{T} and \mathcal{T}' are different but close to each other is in favor of existence of a critical point \mathcal{K} on the line \mathcal{ST}' (similar to the point \mathcal{T} on the line \mathcal{LO}) below which the phase transition from the helical to the LOFF-type state becomes a weakly first order transition.

VI. CURRENT AND ELECTROMAGNETIC RESPONSE IN THE HELICAL STATE

A. The absence of the equilibrium current in the helical ground-state

The oscillating space-dependence of the order parameter like given by Eq. (16) may lead to the hypothesis of a nonzero background electric current present in such a state. We will show here by general arguments that the electric current is in fact absent in the helical state: the condition of its vanishing is equivalent to the minimum of the free energy with respect to the variation of the structure’s wavevector Q .

The superconducting current can be written in the following form:

$$\begin{aligned} \vec{j}_s &= \frac{e}{2} T \sum_{\omega, \mathbf{p}, \lambda} \left(\frac{\partial \epsilon_{\lambda, \mathbf{p}+\mathbf{Q}/2}}{\partial \mathbf{p}} G_{\lambda\lambda}(\omega, \mathbf{p} + \mathbf{Q}/2) - \right. \\ &\quad \left. - \frac{\partial \epsilon_{\lambda, -\mathbf{p}+\mathbf{Q}/2}}{\partial \mathbf{p}} G_{\lambda\lambda}(-\omega, -\mathbf{p} + \mathbf{Q}/2) \right), \end{aligned} \quad (71)$$

where

$$G_{\lambda\lambda}(\omega, \mathbf{p} + \mathbf{Q}/2) = -\frac{i\omega + \epsilon_{\lambda, -\mathbf{p}+\mathbf{Q}/2}}{\tilde{\omega}^2 + \xi_{\lambda}^2 + \Delta^2} \quad (72)$$

is the electron Green’s function in the helical state; $\epsilon_{\lambda, \mathbf{p}}$ is the spectrum of the free electron. For brevity we used notations

$$\tilde{\omega} = \omega + i \frac{\epsilon_{\lambda, \mathbf{p}+\mathbf{Q}/2} - \epsilon_{\lambda, -\mathbf{p}+\mathbf{Q}/2}}{2},$$

$$\xi_{\lambda} = \frac{\epsilon_{\lambda, \mathbf{p}+\mathbf{Q}/2} + \epsilon_{\lambda, -\mathbf{p}+\mathbf{Q}/2}}{2}.$$

The thermodynamic potential in the helical state

$$\Omega_{hel} = -\frac{T}{2} \sum_{\omega, \mathbf{p}, \lambda} \log [\tilde{\omega}^2 + \xi_\lambda^2 + \Delta^2] \quad (73)$$

is evaluated explicitly for an arbitrary spectrum $\epsilon_{\lambda, \mathbf{p}}$ of the electron, due to $|\Delta(\vec{r})| = \text{const.}$

The derivative is

$$\begin{aligned} \frac{\partial \Omega_{hel}}{\partial \vec{Q}} = & \\ -\frac{T}{4} \sum_{\omega, \mathbf{p}, \lambda} & \frac{\frac{\partial \epsilon_{\lambda, \mathbf{p} + \mathbf{Q}/2}}{\partial \mathbf{p}} (i\tilde{\omega} + \xi_\lambda) - \frac{\partial \epsilon_{\lambda, -\mathbf{p} + \mathbf{Q}/2}}{\partial \mathbf{p}} (-i\tilde{\omega} + \xi_\lambda)}{\tilde{\omega}^2 + \xi_\lambda^2 + \Delta^2}. \end{aligned} \quad (74)$$

Comparing this stationary condition (74) with the expression for the current (71), we notice

$$\vec{j}_s = \frac{2e}{\hbar} \frac{\partial \Omega_{hel}}{\partial \vec{Q}}. \quad (75)$$

Thus, a direct calculation of the superconducting current \vec{j}_s shows that in any order of α/v_F the current in equilibrium is zero. This result apparently contradicts the statement made by Yip²⁰, who studied basically the same model as the present one, and found a non-zero supercurrent in the presence of a parallel magnetic field. The resolution of this paradox will be presented in Sec. VII below.

B. Electromagnetic response in the helical state

We calculated the electromagnetic response function $\delta j_\alpha / \delta A_\beta = -\frac{e^2}{mc} n_s^{\alpha\beta}$ for the helical state using the standard diagram methods:

$$\begin{aligned} j_x &= \frac{e^2}{c} T \sum_{\omega, \mathbf{p}, \lambda} (G^2 + F^2) \cos^2 \varphi \left(\frac{p}{m} - \lambda \alpha \right)^2 A_x, \\ j_y &= \frac{e^2}{c} T \sum_{\omega, \mathbf{p}, \lambda} (G^2 + F^2) \sin^2 \varphi \left(\frac{p}{m} - \lambda \alpha \right)^2 A_y, \end{aligned} \quad (76)$$

where $G = G(\omega, \mathbf{p} + \mathbf{Q}/2)$ and $F = F(\omega, \mathbf{p} + \mathbf{Q}/2)$ are correspondingly the normal and the anomalous Green's functions in the helical state. We found that

$$n_s^{yy} = 4 \frac{m}{\hbar} \frac{\partial^2 \Omega}{\partial Q^2}, \quad (77)$$

i. e. proportional to the parameter a from the expansion of the thermodynamic potential (61). Thus on the Lifshitz line \mathcal{LT} there is no linear supercurrent in the direction perpendicular to the magnetic field. The component n_s^{xx} does not vanish anywhere in the helical state region and is of the order of n_s of the BCS state:

$$n_s^{xx} = \frac{4m}{\hbar^2} \left(\frac{v_F^2}{2} \Delta \frac{\partial}{\partial \Delta} \left(\frac{1}{\Delta} \frac{\partial \Omega_{hel}}{\partial \Delta} \right) - \frac{\partial^2 \Omega_{hel}}{\partial Q^2} \right). \quad (78)$$

This anisotropic behavior of the superfluid density tensor is in contrast with the one found in the classical LOFF problem, where n_s was shown to vanish in the whole helical state; the difference is probably due to the fact that in our problem the direction of \mathbf{Q} is fixed by the applied field \mathbf{h} , while in the case of a ferromagnetic superconductor it is arbitrary. The obtained behavior of the $n_s^{\alpha\beta}$ tensor indicates a strongly anisotropic electromagnetic response of the surface superconductor near the Lifshitz line \mathcal{LT} .

VII. “WEAKLY HELICAL” PHASE AT LOW MAGNETIC FIELDS

A. Transformation of the uniform BCS state into long-wavelength helical state

The thermodynamic potential of the helical state in the form of Eq. (53) was obtained while neglecting the term αQ small in comparison with the term $v_F Q$ in the energy of the electron. Within this approximation the thermodynamic potential was symmetric under the change $Q \rightarrow -Q$ and hence the expansion (61) contained only even powers of Q . The account for the first-order term in α/v_F in expressions of the type of Eq. (53) leads (see below) to an appearance of the term ηQ in the thermodynamic potential (61). This term results in the transformation of the homogeneous BCS state (situated on the left of the \mathcal{LT} line) into a weakly helical phase with a small wave-vector $|Q_{hel}| = \frac{2\alpha H}{v_F}$, first found in [10] for small values of H . Mathematically, the terms of the order of α/v_F are considered via taking into account the difference in the density of states in Eq. (53): $\nu(\epsilon_F) \rightarrow \nu_\lambda(\epsilon_F)$. Then the second stationary condition (58) is changed noticeably:

$$\frac{\partial \Omega_{hel}}{\partial Q} = \nu(\epsilon_F) T \sum_{\omega, \lambda} \left(\frac{v_F}{2} + \lambda \frac{\alpha}{2} \right) f(H_\lambda, \omega) = 0, \quad (79)$$

where $f(H_\lambda, \omega)$ is defined in Eq.(60). Now the $Q = 0$ solution never (at any $H \neq 0$) provides a minimum for the superconducting energy:

$$\eta = \left. \frac{\partial \Omega_{hel}}{\partial Q} \right|_{Q=0} = \alpha \nu(\epsilon_F) T \sum_{\omega} f(H, \omega) \neq 0, \quad (80)$$

and the expansion of the thermodynamic potential in powers of Q contains the linear term:

$$\Omega_{hel}(Q) = \Omega_{hel}(0) + \eta Q + \tilde{a} Q^2 + \dots, \quad (81)$$

which clearly indicates that the equilibrium wave vector modulating the order parameter on the left of the \mathcal{LT} line is always non-zero, although small as $\alpha/v_F \ll 1$:

$$Q_{hel} = -\frac{\eta}{2\tilde{a}} = -\frac{2\alpha H}{v_F^2} \times \quad (82)$$

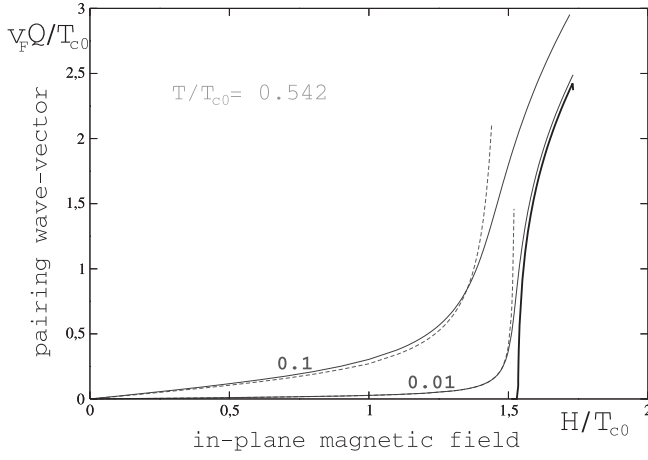


FIG. 7: The dependence of the pairing wave vector Q upon the magnetic field for the two values: $\alpha/v_F = 0.1, 0.01$ (and a particular temperature $T = 0.54T_{c0}$). The curves shown by bold and thin lines correspond to neglecting and taking into account in the SC energy of the helical state the small terms α/v_F . The dashed lines correspond to the approximation (82).

$$\times \frac{\sum_{\omega} \left[\frac{(\omega^2 + H^2 + \Delta^2)}{\mathcal{V}} \mathbf{K}(k) - \mathcal{V} \mathbf{E}(k) \right]}{\sum_{\omega} \left[-\frac{(\omega^2 + \Delta^2)}{\mathcal{V}} \mathbf{K}(k) + \frac{(\omega^2 + \Delta^2)^2 + H^2(\omega^2 - \Delta^2)}{\mathcal{V}(\omega^2 + (H - \Delta)^2)} \mathbf{E}(k) \right]},$$

where k is the Jacobi modulus (59) and $\mathcal{V} = \sqrt{\omega^2 + (H + \Delta)^2}$. In the limit $H \rightarrow 0$ Eq. (82) can be expanded, resulting in the dependence linear in H :

$$Q_{hel} = -2\alpha H/v_F^2. \quad (83)$$

The formula (83) is applicable for small enough magnetic fields; in particular, for $T \approx 0.5T_{c0}$ the field range is limited by $H \leq 0.5T_{c0}$, cf. Fig. 7. At higher fields the dependence of the pairing wave vector upon the magnetic field becomes non-linear but still can be approximated by Eq. (82), until $H \leq 1.3T_{c0}$, cf. Fig. 7. Within the above range of magnetic fields the expansion (81) of the thermodynamic potential is still applicable.

When the magnetic field is further increased, the system approaches the transition into a short-wavelength helical state discussed in Secs. V and VI above. The major role of the small term ηQ is to broaden the \mathcal{LT} line of the second-order transition from the uniform to the helical state into a narrow crossover region. Now the dependence of the pairing wave vector upon the magnetic field should be obtained numerically by solving the system of the two self-consistency equations (55) and (58), while keeping also the term $\propto \alpha/v_F$ via the substitution of $\nu(\epsilon_F)$ by $\nu(\epsilon_F)(1 + \lambda\alpha/v_F)$. The corresponding results for $Q(H)$ are shown by full thin lines in Fig. 7 for two values of α/v_F .

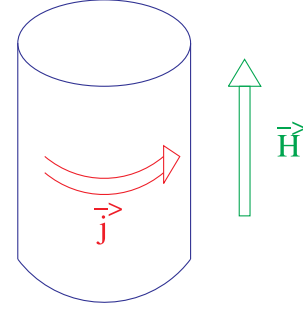


FIG. 8: A superconducting film wrapped in a cylinder (cyclic boundary conditions). This geometrical configuration enables a current to flow in equilibrium in the ground state of the helical phase when a parallel to the axis magnetic field is applied.

B. Cancellation of the ground-state current and a spin-orbital analog of Little-Parks oscillations

The gradient of the phase of the condensate wave function determines the density of the superconducting current

$$\mathbf{j}_s^{(1)} = \frac{e\hbar}{2m} n_s \vec{Q}_{hel}, \quad (84)$$

where n_s is the density of the number of superconducting electrons, $e = -|e|$ is the charge of the electron, and m is the electron true mass. The expansion of Eq. (77) for weak magnetic fields gives $n_s^{yy} = \frac{mv_F^2}{\hbar} \nu(\epsilon_F)(1 - Y(T, \Delta))$. In this limit the density of the current in y -direction, induced by the superconducting phase gradient, reads

$$j_y^{(1)} = -e\nu(\epsilon_F)\alpha(1 - Y(T, \Delta))H. \quad (85)$$

The supercurrent given by Eq. (85) is not the only contribution to be considered. In fact, Yip²⁰ have considered the same model and found that a weak current proportional and perpendicular to the magnetic field flows in the uniform BCS state. Indeed, a calculation of the current in the BCS state gives a non-zero value (coinciding with that in [20])

$$j_y^{(2)} = T \sum_{\omega, \mathbf{p}, \lambda} G_{\lambda}(\omega, \mathbf{p}) \hat{j}_y^{(chir)} = e\nu(\epsilon_F)\alpha(1 - Y(T, \Delta))H. \quad (86)$$

This second contribution leads to the presence (due to the Rashba term in the Hamiltonian) of the anomalous contribution to the electric current.

In the true ground-state with the weak helical modulations, both contributions to the current, Eqs. (85, 86) sum up to produce a perfect zero: $j_y^{(1)} + j_y^{(2)} = 0$, as they should do according to the general proof given in Sec. VIA above. Thus we see the resolution of the controversy with the result [20]: a uniform BCS state considered by Yip does produce a supercurrent under the action of a parallel magnetic field, but this state is *not* the ground-state. Instead, the ground-state is realized as

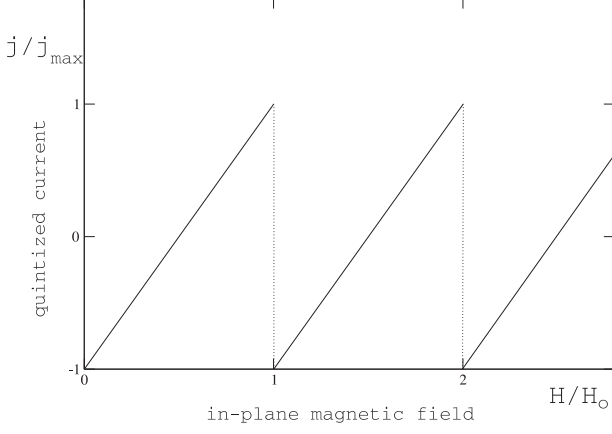


FIG. 9: The sawtooth dependence of the superconducting current j , flowing around a cylinder, upon the magnetic field H . The amplitude is $j_{max} = \frac{e\hbar}{2m}n_s/R$, where R is the cylinder radius. The period is $H_o = \hbar v_F^2/(2\alpha R)$. The strictly linear dependence, shown on the figure, takes place in the case $H_o \ll T_{c0}$, $T = 0$ only.

a weakly helical state with a zero current. In fact, when a parallel magnetic field is applied, the current does not flow, but a phase difference $\Delta\chi = LQ_{hel}$ is induced at the edges of the superconducting film in transverse to the field direction.

However, interesting “traces” of the spin-orbit-induced supercurrent could possibly be seen, if the superconductor is wrapped in a cylinder and a magnetic field is applied along the axis. Then a current may flow around the cylinder (see Fig. 8), due to the quantization condition $\delta\chi = 2\pi n$, $n = 0, \pm 1, \pm 2, \dots$, which does not allow an arbitrary phase shift along the closed loop which encircles the cylinder. The total current will be given by a sum of the “spin-orbit current” $\mathbf{j}_s^{(2)}$ and the current due to the gradient of the quantized phase:

$$j_{quant} = \frac{e\hbar}{2m}n_s \left(-Q_{hel} + \frac{2\pi n}{2\pi R} \right),$$

where R is the cylinder radius and $Q_{hel} = -2\alpha H/v_F^2$. The integer number n is determined as a function of the magnetic field in a way to minimize the current: $n = \text{integer part of } [H/H_o]$, where $H_o = \frac{v_F^2}{2\alpha R}$. The current will vanish at the field values $H = nH_o$, $n = 0, \pm 1, \pm 2, \dots$ only. The maximal value of the current is equal (at $T = 0$) to $j_{max} = \frac{e\hbar}{2m}n_s/R$. The dependence of the current on the magnetic field is of the sawtooth form, as shown in Fig. 9, in the ideal case of zero temperature and absence of impurities. The predicted oscillations of the current are, on first sight, similar to the well-known oscillations in a superconducting cylinder (with the period $B_{LP} = \hbar c/eR^2$ in terms of a real magnetic induction), which goes back to the early stages of the superconductivity studies.²¹ However, the correspond-

ing oscillation periods differ by orders of magnitude: $H_o/H_{LP} \sim (v_F/\alpha) \cdot (k_F R) \gg 1$. We note also, that in a real experiment it should not be necessary the superconducting film to be wrapped in a cylinder; it would be sufficient to fabricate a heterostructure where a thin film with a SO coupling would serve as a weak link introduced into a SQUID-type loop, which would allow to control the superconducting phase difference between the film edges.

VIII. PHASE DIAGRAM IN THE PRESENCE OF NON-MAGNETIC IMPURITIES

In this Section we study the effects of potential impurities upon the superconductive instability in the presence of the Rashba term and the parallel magnetic field. We consider a standard model of short-range weak impurities with a potential $u(\mathbf{r}) = u\delta(\mathbf{r})$ and density n_{imp} ; they are characterized by an elastic scattering time τ , where $\tau^{-1} = 2\pi n_{imp}u^2\nu(\epsilon_F)$. It is assumed that the impurity scattering rate is weak with respect to the Rashba splitting, $1/\tau \ll \alpha p_F$, whereas it can be both weak or strong in comparison with T_c .

The interaction between the electrons and the impurity is described by the following Hamiltonian written in the chiral representation:

$$\hat{H}_{int} = \frac{1}{V} \sum_i \sum_{\mathbf{p}, \mathbf{p}'} u e^{-i(\mathbf{p}-\mathbf{p}')\mathbf{R}_i} a_{\mathbf{p}\lambda}^+ M_{\lambda\mu}(\mathbf{p}, \mathbf{p}') a_{\mathbf{p}'\mu}, \quad (87)$$

where the matrix

$$M_{\lambda\mu}(\mathbf{p}, \mathbf{p}') = \frac{1}{2} \left(1 + \lambda\mu e^{i(\varphi_{\mathbf{p}} - \varphi_{\mathbf{p}'})} \right) \quad (88)$$

appears due to the transformation from the spin to chiral basis. The semiclassical electron Green’s function of the chiral metal in the presence of non-magnetic impurities is

$$G_{\lambda}(\omega, \mathbf{p}) = \frac{1}{i\omega - \xi_{\lambda}(\mathbf{p}) - \lambda H \sin \varphi_{\mathbf{p}} + \frac{i}{2\tau} \text{sgn} \omega}, \quad (89)$$

where $\xi_{\lambda}(\mathbf{p})$ is determined in (22).

The electron-electron vertex in the Cooper channel is then given by non-crossing diagrams shown in Fig. 10, where G denotes the Green’s function (89). Note that the chiralities of both electrons which belong to the same “Cooper block” coincide (otherwise, a diagram would be smaller by a factor $(\alpha p_F \tau)^{-1} \ll 1$).

An analytical expression for the impurity line is (cf. Eq. (88) for the matrix elements)

$$V_{\lambda\mu}(\varphi_{\mathbf{p}}, \varphi_{\mathbf{p}'}) = \frac{1}{8\pi\tau\nu(\epsilon_F)} (1 + \lambda\mu e^{i\varphi_{\mathbf{p}} - i\varphi_{\mathbf{p}'}})^2 = \quad (90)$$

$$\frac{1}{4\pi\tau\nu(\epsilon_F)} e^{i\varphi_{\mathbf{p}} - i\varphi_{\mathbf{p}'}} (\lambda\mu + \sin \varphi_{\mathbf{p}} \sin \varphi_{\mathbf{p}'} + \cos \varphi_{\mathbf{p}} \cos \varphi_{\mathbf{p}'}),$$

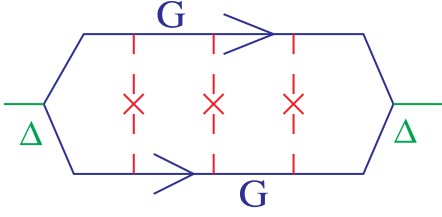


FIG. 10: The electron-electron vertex in the Cooper channel in the presence of non-magnetic impurities.

where λ and μ are the chiralities of the left and the right blocks around the impurity line. In fact, the last term in the r.h.s. of Eq. (90) can be safely omitted since its contribution vanishes after integration over the momenta in the product of $V_{\lambda\mu}$ and the Cooper block, Eq. (91) below. Integrating over ξ_λ a block of two Green's functions (a "Cooper block") in the Cooper channel gives

$$\begin{aligned} C_\lambda(\omega, \sin \varphi_{\mathbf{p}}) &= \\ &= \nu_\lambda(\epsilon_F) \int_{-\infty}^{\infty} d\xi G_\lambda\left(\omega, \mathbf{p} + \frac{\mathbf{q}}{2}\right) G_\lambda\left(-\omega, -\mathbf{p} + \frac{\mathbf{q}}{2}\right) = \\ &= \frac{i\pi\nu_\lambda(\epsilon_F)}{i\bar{\omega} - H_\lambda \sin \varphi_{\mathbf{p}}}, \end{aligned} \quad (91)$$

where $\bar{\omega} = \omega + \text{sgn}\omega/2\tau$, H_λ is determined in (27) and $\nu_\lambda(\epsilon_F) = \nu(\epsilon_F)(1 + \lambda\alpha/v_F)$.

The superconductive transition temperature is determined by the usual condition $U(0)^{-1} = \mathcal{C}$, where \mathcal{C} is the sum of all ladder diagrams with $n = 0, 1, 2, \dots$ impurity lines (see Fig. 10):

$$\begin{aligned} \mathcal{C} &= T \sum_{\omega>0} \sum_{n=0}^{\infty} \sum_{\lambda_n} \int_0^{2\pi} \frac{d\varphi_{\mathbf{p}_n}}{2\pi} L_{\lambda_n}^n(\omega, \varphi_{\mathbf{p}_n}) \times \\ &\quad \times C_{\lambda_n}(\omega, \sin \varphi_{\mathbf{p}_n}) \lambda_n e^{i\varphi_{\mathbf{p}_n}}, \end{aligned} \quad (92)$$

where $L_{\lambda_n}^n(\omega, \varphi_{\mathbf{p}_n})$ is the expression for a ladder diagram which includes a left vertex $L_{\lambda_0}^0(\omega, \varphi_{\mathbf{p}_0}) \equiv \lambda_0 e^{-i\varphi_{\mathbf{p}_0}}$, n "Cooper blocks" and n impurity lines; the factor $\lambda_n e^{i\varphi_{\mathbf{p}_n}}$ corresponds to the right vertex of the diagram in Fig. 10.

In order to sum up the whole Cooper ladder, it is useful to employ a recurrent relation between the ladder diagrams of the n -th and the $n+1$ -th order:

$$\begin{aligned} L_{\lambda_{n+1}}^{n+1}(\omega, \varphi_{\mathbf{p}_{n+1}}) &= \sum_{\lambda_n} \int \frac{d\varphi_{\mathbf{p}_n}}{2\pi} L_{\lambda_n}^n(\omega, \varphi_{\mathbf{p}_n}) \times \\ &\quad \times C_{\lambda_n}(\omega, \sin \varphi_{\mathbf{p}_n}) V_{\lambda_n \lambda_{n+1}}(\varphi_{\mathbf{p}_n}, \varphi_{\mathbf{p}_{n+1}}). \end{aligned} \quad (93)$$

The form of Eq. (90) helps to identify an Ansatz

$$L_{\lambda_n}^n(\omega, \varphi_{\mathbf{p}_n}) = \{l_n^0(\lambda_n, \omega) + l_n^1(\lambda_n, \omega) \sin \varphi_{\mathbf{p}_n}\} e^{-i\varphi_{\mathbf{p}_n}} \quad (94)$$

for the solution which is consistent with the recurrent relation (93). After substituting the Ansatz (94) in Eq. (93), we encounter integrals

$$I_\lambda^j = \frac{1}{4\tau} \int_0^{2\pi} \frac{d\varphi}{2\pi} \frac{i \sin^j \varphi}{i\bar{\omega} - H_\lambda \sin \varphi}, \quad \text{where } j = 0, 1, 2. \quad (95)$$

Then equation (93) can be rewritten in the matrix form

$$\vec{l}_{n+1} = \hat{R} \vec{l}_n, \quad (96)$$

where we define a 4-vector

$$\vec{l}_n^T = (l_n^0(+), l_n^1(+), l_n^0(-), l_n^1(-)) \quad (97)$$

and a 4×4 matrix

$$\hat{R} = \begin{pmatrix} I_+^0 & I_+^1 & -I_-^0 & -I_-^1 \\ I_+^1 & I_+^2 & I_-^1 & I_-^2 \\ -I_+^0 & -I_+^1 & I_-^0 & I_-^1 \\ I_+^1 & I_+^2 & I_-^1 & I_-^2 \end{pmatrix}, \quad (98)$$

with the three "block integrals", Eq. (95), calculated as

$$\begin{aligned} I_\lambda^0 &= \frac{1}{\sqrt{\bar{\omega}^2 + H_\lambda^2}} \frac{1}{4\tau}, \\ I_\lambda^1 &= \frac{i}{H_\lambda} \left(\frac{|\bar{\omega}|}{\sqrt{\bar{\omega}^2 + H_\lambda^2}} - 1 \right) \frac{1}{4\tau}, \\ I_\lambda^2 &= -\frac{|\bar{\omega}|}{h_\lambda^2} \left(\frac{|\bar{\omega}|}{\sqrt{\bar{\omega}^2 + H_\lambda^2}} - 1 \right) \frac{1}{4\tau}. \end{aligned} \quad (99)$$

Now we can proceed with the calculation of the Cooper ladder. We substitute the Ansatz (94) and the Cooper block (91) in the Cooper ladder (92), and obtain

$$\begin{aligned} \mathcal{C} &= 4\pi\tau\nu(\epsilon_F)T \sum_{\omega>0} \sum_{n=0}^{\infty} \sum_{\lambda} \lambda (l_n^0(\lambda) I_\lambda^0 + l_n^1(\lambda) I_\lambda^1) = \\ &= 4\pi\tau\nu(\epsilon_F)T \sum_{\omega>0} \vec{l}^T \cdot (1 - \hat{R})^{-1} \cdot \vec{l}_0, \end{aligned} \quad (100)$$

where we used the definition of the integrals (95) and the 4-vectors (97), and we summed up the geometric progression $\sum_{n=0}^{\infty} \hat{R}^n = (1 - \hat{R})^{-1}$. We also introduced a vector $\vec{l}^T = (I_+^0, I_+^1, -I_-^0, -I_-^1)$ and used a notation $\vec{l}_0^T = (1, 0, -1, 0)$, corresponding to the definition of $L_{\lambda_0}^0(\omega, \varphi_{\mathbf{p}_0})$. At this point we have as well neglected the difference $\nu_+ \neq \nu_-$.

Evaluating the scalar product in Eq. (100), we find the Cooper ladder \mathcal{C} and the equation for T_c :

$$\frac{1}{\nu(\epsilon_F)U(0)} = \pi T \max_q \sum_{\omega>0} K\left(\omega, H_+, H_-, \frac{1}{2\tau}\right), \quad (101)$$

where the kernel is

$$K(\omega) = 4\tau \frac{(I_+^0 + I_-^0) [1 - (I_+^2 + I_-^2)] + (I_+^1 - I_-^1)^2}{(1 - (I_+^0 + I_-^0)) [1 - (I_+^2 + I_-^2)] - (I_+^1 - I_-^1)^2}. \quad (102)$$

Equation (101) for $T_c(h)$ was solved numerically; the phase transition lines are shown in Fig. 11 for a number of impurity scattering strengths $1/2\tau T_{c0}$, interpolating from a clean to dirty limit. It is seen that in the clean

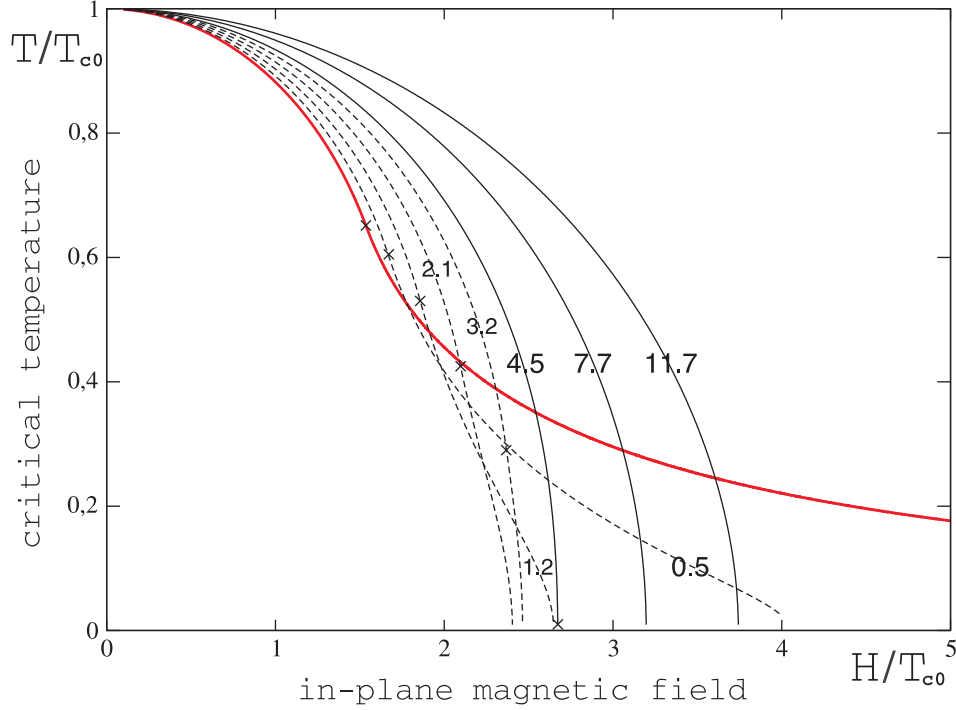


FIG. 11: Phase transition lines for different strengths of impurity scattering: $1/2\tau T_{c0} = 0.0, 0.5, 1.2, 2.1, 3.2, 4.5, 6.0, 7.7, 9.6, 11.7$. Lifshitz points are shown by crosses.

limit $T_{c0}\tau \gg 1$ the impurity scattering decreases the critical parallel magnetic field (in the clean limit it is given by $H_{p0} = \sqrt{2\alpha p_F \Delta(0)}$ first found in [4]) and simultaneously pushes the position of the \mathcal{L} point to higher values of H and lower values of T . As a result, both short-wavelength inhomogeneous states disappear from the phase diagram at $\tau^{-1} \geq 9T_{c0}$. Note a large numerical factor 9 which enters the definition of the “dirty” regime in the present problem. In the “dirty limit” $1/\tau \geq 10T_{c0}$ the kernel $K(\omega)$ simplifies to

$$K(\omega) = \frac{2}{|\omega| + 2H^2\tau + v_F^2 Q^2 \tau / 4}. \quad (103)$$

The kernel (103) is maximal at $Q = 0$, i. e. in the dirty limit one obtains a homogeneous superconducting phase (see below, however). The zero-temperature limit of the paramagnetic critical magnetic field $H_p(0)$ can be easily obtained with the use of Eq. (103) as

$$H_p = \sqrt{\frac{\pi T_{c0}}{4\tau e\gamma}}. \quad (104)$$

Thus, in the dirty limit $1/\tau \gg T_{c0}$ the paramagnetic critical field *grows* with increase of disorder.

The above results in this Section were obtained in the main order over the parameter α/v_F . The linear in α/v_F terms can be included in the same way it was done in the preceding Section, which lead to the substitution of $I_\lambda^j \rightarrow I_\lambda^j(1 + \lambda\alpha/v_F)$ in the kernel (102). Then in the

dirty limit the kernel reads

$$K(\omega) = \frac{2}{|\omega| + 2H^2\tau + v_F^2 Q^2 \tau / 4 + 2\tau\alpha QH}. \quad (105)$$

Maximization of the Cooper loop with the kernel (105) with respect to the pairing vector Q leads to a non-zero momentum of the Cooper pair, equal to

$$Q_{hel} = -\frac{4\alpha H}{v_F^2}, \quad (106)$$

for all values of the magnetic field. Thus the terms α/v_F transform the homogeneous superconducting state into a weakly inhomogeneous helical state, analogously to the clean case. Note, that the small wave vector modulating the order parameter in the “dirty” limit, Eq. (106), is twice larger than it is in the clean case for weak magnetic fields, Eq. (83). Note, however, that the result (106) was obtained near the transition line $T_c(H)$ only.

IX. FLUCTUATIONAL EFFECTS NEAR THE $T_c(H)$ TRANSITION LINE

The corrections to the mean-field approximation, employed in this paper, are usually of the order of T_c/ϵ_F for a clean 2D superconductor: the actual transition is of the Berezinsky-Kosterlitz-Thouless vortex depairing type, and the transition temperature is shifted downwards by a relative amount $T_c/\epsilon_F \ll 1$. In our system

the fluctuations are enhanced strongly around the special points \mathcal{L} and \mathcal{S} , where an additional analysis is needed.

We start from the \mathcal{L} point and recall that near the whole \mathcal{LT} line the component n_s^{yy} of the superfluid density is suppressed, cf. Eq. (77), proportionally to the coefficient a from Eq. (62). Within the approximation used in Sec. VI and above, this reduction factor could be arbitrary small, since n_s^{yy} vanishes exactly at the \mathcal{LT} line. However, as it was explained in Sec. VII A, an account of the sub-leading terms $\propto \alpha/v_F$ transforms the \mathcal{LT} line of the Lifshitz phase transition into a crossover region. The minimal value of the second derivative $d^2\Omega_{hel}(Q)/dQ^2$ and thus of the ratio n_s^{yy}/n_s^{xx} then scales as $\eta^{2/3} \propto (\alpha/v_F)^{2/3}$. In a superconductor with an anisotropic tensor of the superfluid density, the effective “rigidity modulus” is controlled by the geometric average $\sqrt{n_s^{xx}n_s^{yy}}$. The strength of the phase fluctuations is thus larger near the \mathcal{LT} line by a factor $(v_F/\alpha)^{1/3}$. Therefore, the fluctuational reduction of the transition temperature near the \mathcal{L} point is enhanced by the same relative factor $(v_F/\alpha)^{1/3} \gg 1$, cf. Fig. 12.

Another mechanism of a fluctuation enhancement is effective near the \mathcal{S} point due to the extended $U(2)$ symmetry of the order parameter. Exactly at the symmetric point \mathcal{S} the order parameter spinor spans the sphere S^3 and is equivalent to a four component unit vector, see Eq. (35). The thermal fluctuations of the classical $O(N)$ nonlinear vector model in 2D space have been studied by Polyakov [22]. On a large length scales $L \gg \xi(T)$, where $\xi(T)$ is the temperature-dependent superconductive correlation length, the evolution of the dimensionless coupling constant $g = T \left(\frac{\hbar^2}{2m} n_s \right)^{-1}$ is governed (for $N = 4$) by the renormalization-group equation

$$\frac{dg}{dX} = \frac{2}{\pi} g^2, \quad (107)$$

where $X = \log(L/\xi(T))$. Deviations from the symmetric point are measured (cf. Sec. VI) by the anisotropy parameter β_a which enters into the free energy in the combination

$$\beta_a(T, H) |\Delta|^4 (\mathcal{N}_1^2 + \mathcal{N}_2^2 - \mathcal{N}_3^2 - \mathcal{N}_4^2)^2. \quad (108)$$

It is easy to show the following²²: that the anisotropy parameter β_a satisfies a renormalization group equation:

$$\frac{d\beta_a}{dX} = -\frac{4g}{\pi} \beta_a. \quad (109)$$

Running solution of Eqs. (107, 109) can be easily found:

$$g^{-1} = g_0^{-1} - \frac{2}{\pi} X \quad (110)$$

and

$$\beta_a = \beta_a^0 \left(1 - \frac{2g_0}{\pi} X \right)^2 \quad (111)$$

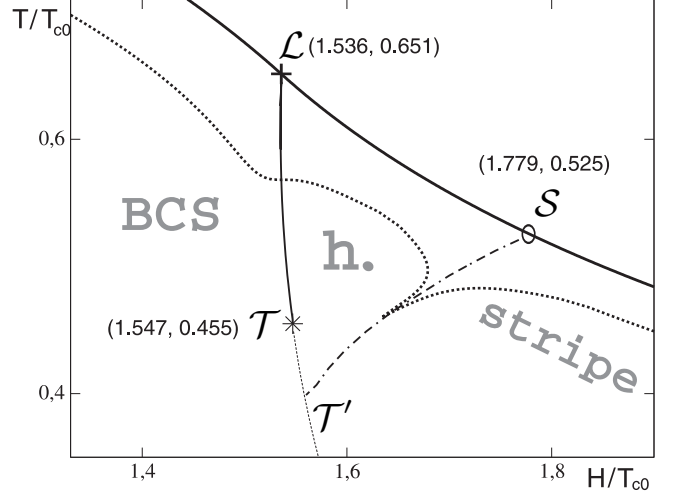


FIG. 12: The phase diagram with the physical $T_{BKT}(H)$ transition line shown by a dotted line, for the values $T_{c0}/\epsilon_F = 0.02$ and $\alpha/v_F = 0.34$. The effect of the enhanced fluctuations in the regions near the points \mathcal{L} and \mathcal{S} is seen as a shift of the $T_{BKT}(H)$ line in the direction of lower temperature and field, with respect to its mean-field position. The mean-field phase transition line $T_c(H)$ is shown by a solid line.

(a renormalization of the coefficient β_s is absent within the same approximation). The infra-red cutoff length $L_{\max}(T)$ for the renormalization flow solution (110, 111) coincides with the length L_{an} defined in Eq. (36). Finally, we obtain the renormalized parameters

$$n_s = n_s^0 - \frac{2Tm}{\pi\hbar^2} \log \left(\frac{\beta_s}{\beta_a} \right) \quad (112)$$

and

$$\beta_a = \beta_a^0 \left(1 - \frac{2Tm}{\pi\hbar^2 n_s^0} \log \left(\frac{\beta_s}{\beta_a} \right) \right)^2. \quad (113)$$

The above formulae are valid as long as the effective renormalization group “charge” $g(X_{\max})$ is small compared to unity; within this domain a strong suppression of β_a is still possible. Qualitatively, the result of the $U(2)$ -fluctuations is twofold: i) the “nearly-isotropic” behavior extends to a wider region around the \mathcal{S} point, and ii) the transition temperature occurs to be additionally suppressed within the same region.

To conclude this Section, fluctuations lead to the deformation of the phase transition line $T_c(H)$ in the vicinities of the \mathcal{L} and \mathcal{S} points, as shown in Fig. 12.

X. CONCLUSIONS

In this paper we found the phase diagram of a surface superconductor with a relatively strong Rashba splitting of the electron spectrum: $T_c \ll \alpha p_F \ll \epsilon_F$, in the presence of a parallel magnetic field, both in clean and disordered cases. In the clean limit, we demonstrated that in

the lowest approximation over the spin-orbital parameter α/v_F the phase diagram is universal and contains the unusual “helical” phase with the order-parameter modulation $\propto \exp(i\mathbf{Q}\mathbf{r})$, as well as a usual BCS-type phase and a LOFF phase with a sinusoidal modulation at higher magnetic fields. The absolute value of the modulation wavevector is typically $Q \sim g\mu_B\hbar/\hbar v_F$. Non-magnetic impurities tend to diminish the region where these modulated phases exist, and eliminate them completely in the dirty limit. Once sub-leading terms of the order of α/v_F (which are due to the different chiral subband DoS) are taken into account, the uniform BCS state becomes unstable and transforms into a “weakly modulated” helical phase with $Q_{\text{slow}} \sim \alpha g\mu_B\hbar/\hbar v_F^2$. A weakly modulated phase is stable with respect to disorder, as its origin can be found in the symmetry of the problem.¹⁰

In the clean limit, we were able to determine the positions of the phase transition lines between the BCS, the helical and the LOFF states on the (H, T) phase diagram. It was found possible to implement this calculation mainly analytically, due to the fact that the absolute value of the order parameter is constant in the helical state. We have shown that the thermal phase fluctuations are enhanced strongly around both these transition lines, leading to local “caves” of the $T_c(h)$ transition line near the end-points \mathcal{L} and \mathcal{S} . We expect that a fluctuational correction to the conductivity of the Aslamazov-Larkin type²³ should be strongly anisotropic near the \mathcal{L} point, which could be one of the signatures of the proposed phase diagram.

We have shown that an electric current does not flow in the equilibrium state of our system at any parallel magnetic field (as long as the system is infinite), contrary to the statement made in [20]. However, if the system is considered in the finite-stripe geometry with the periodic boundary conditions, an oscillating (as a function of the parallel magnetic field) current is expected, which is another special feature of a superconductor with a strong Rashba coupling.

A new type of a vortex-like topological defect was predicted to exist in the region near the special \mathcal{S} point of the phase diagram, due to the extended $U(2)$ order parameter symmetry realized at this point. Contrary to the usual singular vortex, this new topological defect is non-singular in the sense that the amplitude of the order parameter does not vanish in the vortex core. We showed that the energy of the non-singular vortex is lower than that of the singular vortex in some finite region around the \mathcal{S} point. The nature of an elementary vortex defect differs between the helical and the stripe phases (in the regions to the left and to the right from the \mathcal{S} point): whereas in the helical state a vortex carries an integer flux $\Phi = n\Phi_0$ and an integer topological charge $Q = n$, these quantum numbers are *half-integer* in the stripe state. Physically, these half-vortices correspond to the presence of a vortex-like defect within only one (either Δ_+ or Δ_-) component of the order parameter.

Note added.—When this paper was nearly completed,

we learned about a recent preprint by Agterberg and Kaur²⁴, where the density of states effects (due to $\nu_+ \neq \nu_-$) upon the phase diagram of the Rashba superconductor were studied in the clean limit by means of a numerical solution of the Eilenberger equations. The main emphasis was made on the 3-dimensional systems there, thus the comparison is not straightforward. Qualitatively, the results they obtained seem to be in agreement with ours.

Acknowledgments

We thank Yu. S. Barash, V. B. Geshkenbein, L. B. Ioffe, A. B. Kashuba, V. P. Mineev, P. M. Ostrovsky, H. R. Ott, D. A. Ivanov, M. Sigrist, M. A. Skvortsov, A. M. Tsvelik, K. S. Turitsyn, G. E. Volovik for many useful discussions. This research was supported by SCOPES grant, RFBR grants 01-02-17759, 04-02-16348 and 04-02-08159, and Program “Quantum macrophysics” of Russian Academy of Sciences. The research of O. D. was also supported by the Dynasty Foundation and the Landau Scholarship (FZ-Juelich).

APPENDIX

1. Transformation to elliptic integrals

Consider the integral

$$I_1 = \int_0^{2\pi} \frac{d\varphi}{2} \frac{1}{\sqrt{(\omega + iH_\lambda \sin \varphi)^2 + \Delta^2}}, \quad (114)$$

which enters Eq. (55), and note that $\int_0^{2\pi} f(\sin \varphi) d\varphi = 4 \int_0^{\pi/2} f(\cos 2\varphi) d\varphi$ for any function f . Using then the identity $\cos 2\varphi = \cos^2 \varphi - \sin^2 \varphi$ and the substitution $\varphi = \arctan t$, we transform Eq. (114) into

$$I_1 = 2 \int_0^\infty \frac{dt}{\sqrt{Ae^{i\psi}t^4 + 2(\omega^2 + H_\lambda^2 + \Delta^2)t^2 + Ae^{-i\psi}}}, \quad (115)$$

where we denoted $Ae^{i\psi} = (\omega - iH_\lambda)^2 + \Delta^2$, and

$$A = \sqrt{(\omega^2 + (|H_\lambda| + \Delta)^2)(\omega^2 + (|H_\lambda| - \Delta)^2)}. \quad (116)$$

The integral (115) is rapidly convergent, thus it is possible to make a transformation of variables in the complex plane $\tau = te^{i\frac{\psi}{2}}$ and to reduce Eq. (115) to

$$I_1 = 2 \int_0^\infty \frac{d\tau}{\sqrt{A}\sqrt{1 + (a + a^{-1})\tau^2 + \tau^4}}, \quad (117)$$

where

$$a = \sqrt{\frac{(\omega^2 + (|H_\lambda| + \Delta)^2)}{(\omega^2 + (|H_\lambda| - \Delta)^2)}}. \quad (118)$$

(in the course of transformation from Eq. (115) to Eq. (117) we rotated the path of integration over τ by the angle $\psi/2$). Making an inverse substitution $\tau = \tan \varphi$ in Eq. (117) gives

$$I_1 = \frac{2}{\sqrt{A}} \int_0^{\pi/2} \frac{d\varphi}{\sqrt{1 + \left(\frac{\sqrt{a}-\sqrt{a^{-1}}}{2}\right)^2 \cos^2 2\varphi}}. \quad (119)$$

Following the definition of an elliptic integral of the first kind $\mathbf{K}(k) = \int_0^{\pi/2} (1 - k^2 \sin^2 \varphi)^{-1/2} d\varphi$, we rewrite Eq. (119) as

$$I_1 = \frac{2}{\sqrt{A}} \mathbf{K} \left(i \frac{\sqrt{a} - \sqrt{a^{-1}}}{2} \right) = \frac{2}{\sqrt{A}} \frac{\mathbf{K} \left(\sqrt{1 - \frac{1}{a^2}} \right)}{\sqrt{a}}. \quad (120)$$

The last expression in (120) leads directly to the gap equation (57), with A and a given by Eqs. (116) and (118).

2. Equation for the \mathcal{ST}' line

Here we present the transformation of Eq. (68), which determines the helical state metastability line \mathcal{ST}' , to the complete elliptic integrals of the first and the third kind (\mathbf{K} and $\mathbf{\Pi}$):

$$I_2 = \int_0^{2\pi} d\varphi \frac{1}{4\sqrt{\tilde{\omega}^2 + \Delta^2}} \frac{-1 + (\tilde{\omega} + iX \sin \varphi)^2}{\tilde{\omega}^2 + \Delta^2 + (X \sin \varphi)^2} = \frac{z\mathbf{K}(k) - z_1\mathbf{\Pi}(l_1, k) - z_2\mathbf{\Pi}(l_2, k)}{\sqrt{(\Delta + H)^2 + \omega^2}} \quad (121)$$

and

$$I_3 = \int_0^{2\pi} \frac{1}{4\sqrt{\tilde{\omega}^2 + \Delta^2}} \frac{\Delta^2}{\tilde{\omega}^2 + \Delta^2 + (X \sin \varphi)^2} = \frac{y\mathbf{K}(k) - y_1\mathbf{\Pi}(l_1, k) - y_2\mathbf{\Pi}(l_2, k)}{\sqrt{(\Delta + H)^2 + \omega^2}}, \quad (122)$$

where $\tilde{\omega} = \omega + iH \sin \varphi$. In Eqs. (121, 122) we introduced notations

$$l_1(\mathbf{S}) = 1 - \frac{(\Delta - H + i\omega)(\Delta^2 - (H + i\omega)^2 + X^2)}{(\Delta + H + i\omega)(\Delta^2 + H^2 + \omega^2 - X^2 - 2i\mathbf{S})},$$

$$l_2(\mathbf{S}) = l_1(-\mathbf{S});$$

$$z = -2 - \frac{\Delta H(2i\omega X + \Delta(H + 2X))}{(\Delta + i\omega)^2 X^2},$$

$$z_1(\mathbf{S}) = -\frac{(\Delta - H + i\omega) L(\mathbf{S})}{2(\Delta + i\omega)^2 X^2 (\Delta^2 - (H - i\omega)^2 + X^2) \mathbf{S}},$$

$$z_2(\mathbf{S}) = z_1(-\mathbf{S});$$

$$y = \frac{\Delta^2 H^2}{(\Delta + i\omega)^2 X^2},$$

$$y_1(\mathbf{S}) = -\frac{i\Delta^2 (\Delta - H + i\omega) M(\mathbf{S})}{2(\Delta + i\omega)^2 X^2 (\Delta^2 - (H - i\omega)^2 + X^2) \mathbf{S}},$$

$$y_2(\mathbf{S}) = y_1(-\mathbf{S}); \quad (123)$$

where

$$L(\mathbf{S}) = -i\Delta^4 H(H + X)^2 -$$

$$- 2\omega^2 X^2 (H - i\omega + X)(\omega X + \mathbf{S}) +$$

$$+ 2i\Delta\omega X(H + X)(H - i\omega + X)(\omega X + \mathbf{S}) +$$

$$+ \Delta^3 (H + X)^2 (-iH^2 - H\omega + 2\omega X + iX^2 + \mathbf{S}) +$$

$$+ \Delta^2 (H + X)(H^2 - iH\omega + HX + i\omega X)(2\omega X + \mathbf{S}) -$$

$$- \omega X^2 \Delta^2 (H + X)^2,$$

$$\mathbf{S} = \sqrt{-\Delta^2 H^2 + (\Delta^2 + \omega^2) X^2}, \quad X = \frac{q + Q}{2}; \quad (124)$$

$$M(\mathbf{S}) = \Delta H^3 (\Delta + H - i\omega) -$$

$$- HX^2 (\Delta(\Delta + 2H) - i(\Delta - H)\omega + 2\omega^2) +$$

$$+ (\Delta + i\omega)X^4 +$$

$$+ (H^2(i(\Delta + H) + \omega) + (-i(\Delta + H) + \omega)X^2) \mathbf{S}. \quad (125)$$

3. The eighth order terms in the Ginzburg-Landau functional

Here we present a calculation of the coefficient κ which is in front of the eighth-order anisotropic term in the free energy, Eq. (70). As it was mentioned, the sign of κ determines the type of the helical state instability.

The terms of the eighth order in Δ in the Ginzburg-Landau functional are

$$F_{sn}^{(8)} = \frac{a}{8} \Delta^8 + \frac{b}{8} (|u|^2 - |v|^2)^2 \Delta^4 +$$

$$\frac{(D_1 - D_2 + D_3/2)}{8} (|u|^2 - |v|^2)^4 + E_{3Q}, \quad (126)$$

where all but the last term originate from the expansion of the free energy in powers of the basic amplitudes u and v , and notations $a = D_1 + D_2 + D_3/2$ and $b = 6D_1 - D_3$ are introduced. The last term E_{3Q} arises due to the nonlinearity-induced additional harmonics with momenta $\pm 3Q$ and amplitudes $u_{\pm 3Q}$ and $v_{\pm 3Q}$; explicit form of E_{3Q} will be specified shortly. Actually we are interested in terms which contribute to the coefficient κ in front of the $\cos^4 \theta$ term in Eq. (70), thus the terms in the first line of Eq. (126) are irrelevant.

The coefficients $D_{1,2,3}$ come from the 8-vertices diagrams shown in Fig. 13. The corresponding analytical expressions are summarized below (we introduce notations $D_i = T \sum_{\omega, \mathbf{p}, \lambda} \tilde{D}_i$):

$$\begin{aligned}
\tilde{D}_1 &= \frac{1}{8} G_{p+\frac{Q}{2}}^4 G_{-p+\frac{Q}{2}}^4, & \tilde{D}_2 &= G_{p+\frac{Q}{2}}^4 G_{-p+\frac{Q}{2}}^3 G_{-p-\frac{3Q}{2}} + G_{p+\frac{Q}{2}}^3 G_{-p+\frac{Q}{2}}^2 G_{-p-\frac{3Q}{2}}^2 G_{p+\frac{5Q}{2}}, \\
\tilde{D}_3 &= \frac{3}{2} G_{p+\frac{Q}{2}}^4 G_{-p+\frac{Q}{2}}^2 G_{-p-\frac{3Q}{2}}^2 + G_{p+\frac{Q}{2}}^3 G_{-p+\frac{Q}{2}} G_{-p-\frac{3Q}{2}}^3 G_{p+\frac{5Q}{2}} + G_{p+\frac{Q}{2}}^3 G_{-p+\frac{Q}{2}}^3 G_{-p-\frac{3Q}{2}} G_{p-\frac{3Q}{2}} + \\
&+ G_{p+\frac{Q}{2}}^2 G_{-p+\frac{Q}{2}}^2 G_{-p-\frac{3Q}{2}}^2 G_{p-\frac{3Q}{2}} G_{p+\frac{5Q}{2}},
\end{aligned} \tag{127}$$

where G are the normal metal Green's functions. The integration is first done over $d\xi = d(p^2/2m - E_F)$, then over $d\varphi$ by means of a generating function $1/\sqrt{\omega^2 + (\lambda H \pm nQ)^2}$, where $n = 1, 3, 5$. The obtained analytical expressions are evaluated for the values $T_S = 1.779T_{c0}$, $H_S = 0.525T_{c0}$ and $Q_S = 2.647T_{c0}$ at the \mathcal{S} point of the $T_c(H)$ line. The summation over ω is performed numerically, resulting in

$$\begin{aligned}
D_1 &= 0.00106053, & D_2 &= 0.00152674, \\
D_3 &= -0.00120067.
\end{aligned} \tag{128}$$

Now we turn to the evaluation of the “induced” term E_{3Q} in the free energy (126). It appears due to a generation of the third harmonics $e^{\pm 3iQ}$ in the order parameter. The amplitudes of the third harmonics u_{3Q} and v_{3Q} are small and proportional to the third power of the basic amplitudes u and v . The “induced” term reads

$$E_{3Q} = \mathcal{V}^+ A \mathcal{V} + (X^+ \mathcal{V} + \mathcal{V}^+ X), \tag{129}$$

where the matrix A and the vector X contain numerical coefficients l_i , which are determined by means of evaluation of the loop diagrams with two, four and six vertices (shown in Fig. 14):

$$A = \begin{pmatrix} l_1 + l_3|u|^2 + l_4|v|^2 & l_5 uv \\ l_5 u^* v^* & l_1 + l_4|u|^2 + l_3|v|^2 \end{pmatrix},$$

$$\begin{aligned}
\mathcal{V}^+ &= (u_{3Q}^*, v_{-3Q}), & X^+ &= (x^*, y), \\
x &= l_2 u^2 v^* + l_6 u^2 v^* |u|^2 + (l_7 + l_8) u^2 v^* |v|^2; \\
y &= l_2 v^2 u^* + l_6 v^2 u^* |v|^2 + (l_7 + l_8) v^2 u^* |u|^2.
\end{aligned} \tag{130}$$

The fifth and higher harmonics, as well as the higher powers of the third harmonics, do not contribute to the eighth order in Δ . The amplitudes u_{3Q} and v_{-3Q} in Eq. (129) are found from the minimization of the superconducting energy: $\frac{\partial E_{3Q}}{\partial \mathcal{V}} = 0$, which gives

$$\begin{aligned}
E_{3Q} &= -X^+ A^{-1} X \equiv \\
d_2 \cdot (|u|^6 |v|^2 + |u|^2 |v|^6) &+ d_3 \cdot |u|^4 |v|^4,
\end{aligned} \tag{131}$$

where

$$\begin{aligned}
d_2 &= \frac{l_2(-2l_6 l_1 + l_2 l_3)}{l_1^2} \\
d_3 &= \frac{2l_2(-2(l_7 + l_8)l_1 + l_2(l_4 + l_5))}{l_1^2}.
\end{aligned} \tag{132}$$

The analytic expressions for the diagrams shown in Fig. 14 are (we introduce notations $l_i = T \sum_{\omega, \mathbf{p}, \lambda} \tilde{l}_i$)

$$\begin{aligned}
l_1 &= \frac{1}{U} - \frac{T}{2} \sum_{\omega, \mathbf{p}, \lambda} G_{p+\frac{3Q}{2}} G_{-p+\frac{3Q}{2}}, \\
\tilde{l}_2 &= \frac{1}{2} G_{p+\frac{Q}{2}} G_{-p+\frac{Q}{2}} G_{-p-\frac{3Q}{2}} G_{p+\frac{5Q}{2}}, \\
\tilde{l}_3 &= G_{-p+\frac{Q}{2}} G_{p-\frac{3Q}{2}}^2 G_{-p-\frac{3Q}{2}}, \\
\tilde{l}_4 &= G_{-p+\frac{5Q}{2}} G_{p-\frac{3Q}{2}}^2 G_{-p-\frac{3Q}{2}}, \\
\tilde{l}_5 &= G_{-p+\frac{Q}{2}} G_{p-\frac{3Q}{2}} G_{-p-\frac{3Q}{2}} G_{p+\frac{5Q}{2}}, \\
\tilde{l}_6 &= G_{p+\frac{Q}{2}} G_{-p+\frac{Q}{2}}^2 G_{p-\frac{3Q}{2}} G_{-p-\frac{3Q}{2}}, \\
\tilde{l}_7 &= \frac{1}{2} G_{p+\frac{Q}{2}}^2 G_{-p+\frac{Q}{2}}^2 G_{p-\frac{3Q}{2}} G_{-p-\frac{3Q}{2}}, \\
\tilde{l}_8 &= G_{p+\frac{5Q}{2}} G_{p+\frac{Q}{2}} G_{-p+\frac{Q}{2}} G_{p-\frac{3Q}{2}} G_{-p-\frac{3Q}{2}}^2.
\end{aligned} \tag{133}$$

The calculation of the above integrals in the symmetric point \mathcal{S} leads to numerical values

$$\begin{aligned}
l_1 &= 0.674254, & l_2 &= 0.103447, \\
l_3 &= 0.191039, & l_4 &= 0.170477, \\
l_5 &= 0.206894, & l_6 &= 0.0325726, \\
l_7 &= 0.00491175, & l_8 &= 0.021198,
\end{aligned} \tag{134}$$

which we substitute in Eq. (132). Finally for the coefficient κ we obtain a positive value:

$$\kappa = D_1 - D_2 + D_3/2 - d_2 + d_3/2 = 0.0053. \tag{135}$$

¹ S. Reich and Y. Tsabba, Eur. Phys. J. B **9**, 1 (1999). Y. Levi et al., Europhys. Lett., **51**, 564 (2000).

² V. M. Edelstein, JETP, **95**, 2151 (1989).

³ L. P. Gor'kov and E. I. Rashba, Phys. Rev. Lett. **87**, 037004 (2001).

⁴ V. Barzykin and L. P. Gor'kov, Phys. Rev. Lett. **89**, 227002

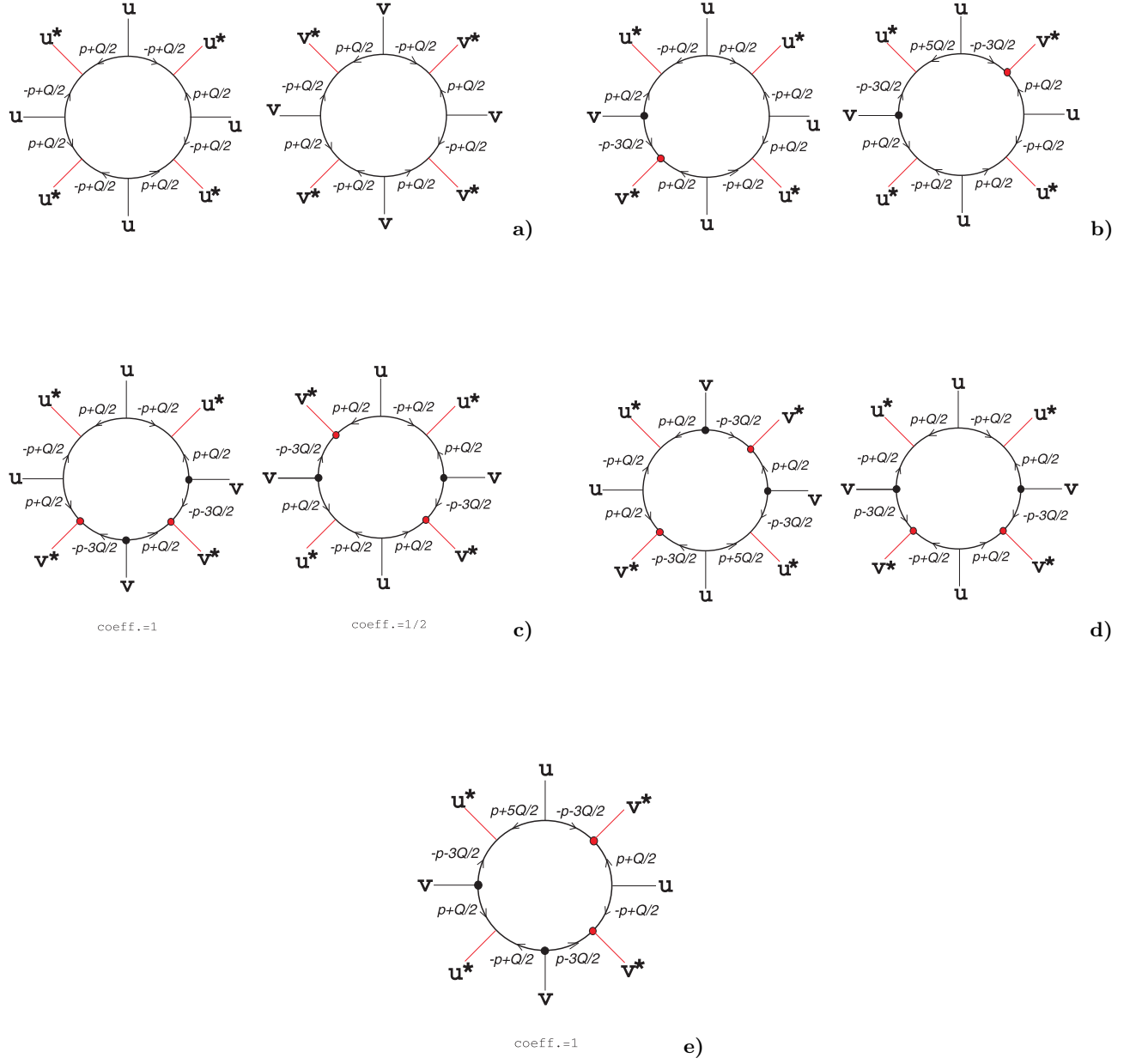


FIG. 13:

a) Diagrams, corresponding to the coefficient D_1 in front of the term $|u|^8 + |v|^8$ in the Ginzburg-Landau expansion. The combinatorial coefficient of the diagrams is $1/8$. All the loops are symmetric under the replacement $Q \rightarrow -Q$, which is equivalent to the replacement $u \rightarrow v$. Therefore all such diagrams are equal.

b) Two different diagrams, which form the coefficient D_2 in front of the term $|v|^2|u|^6$. The combinatorial coefficient of both is equal to 1.

The diagrams **c)**, **d)**, **e)** form the coefficient D_3 in front of the term $|u|^4|v|^4$:

c) two loops with equal values but different combinatorial coefficients 1 and $1/2$ correspondingly. Under the replacement $u \rightarrow v$ both diagrams do not change. The complex conjugate of them simply reverse the encircling along the loop and such diagrams are taken into account in the combinatorial coefficients.

d) the combinatorial coefficient of these both two diagrams is equal to 1, if we keep in mind the complex conjugate of them. The two loops transfer one into another under the replacement $u \rightarrow v$.

e) a diagram with a combinatorial coefficient equal to 1.

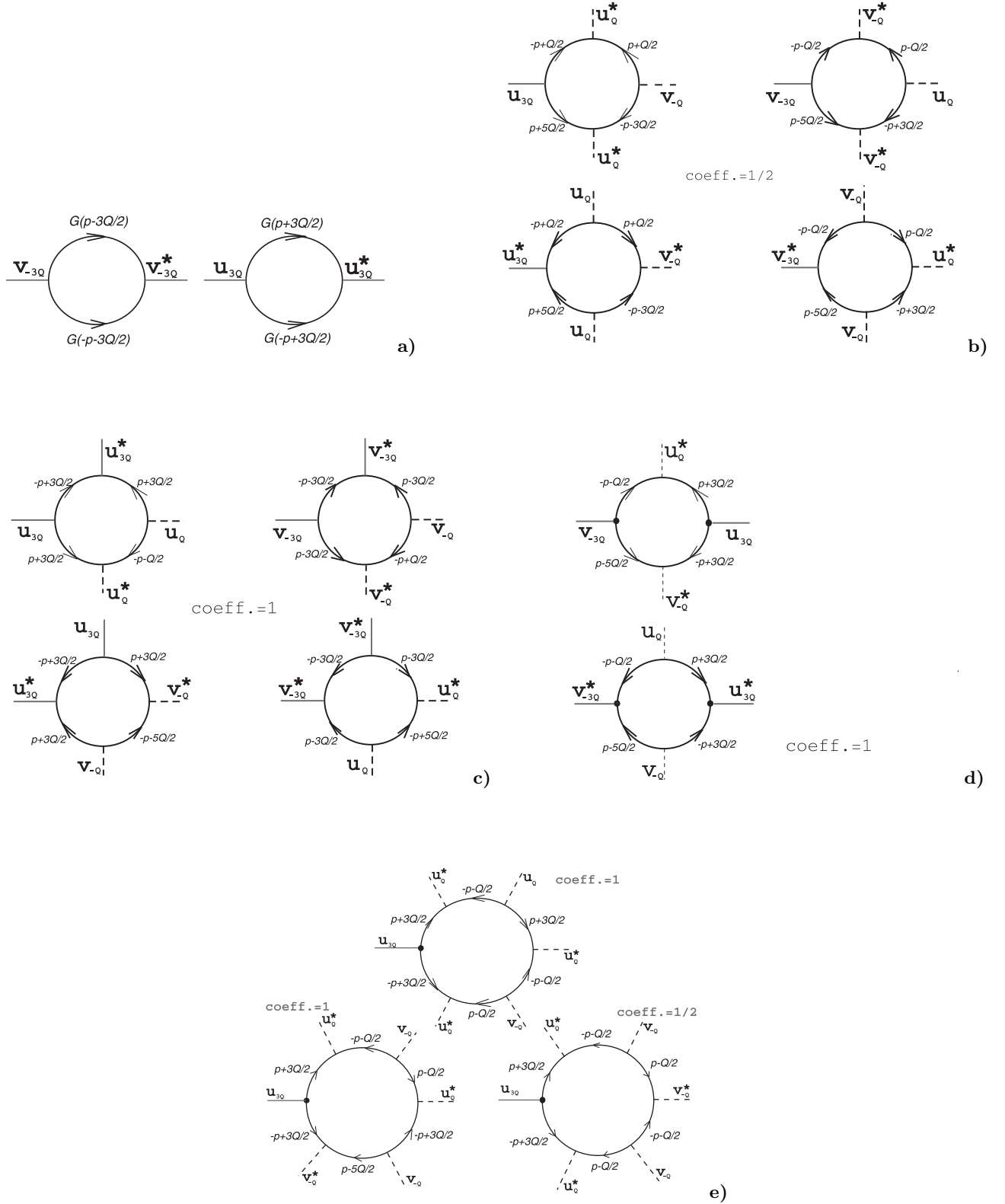


FIG. 14: Diagrams **a)**, **b)** are of the sixth order in u :

a) the Cooper loop for the third harmonic, which corresponds to the coefficient l_1 in the GL expansion; it has a combinatorial coefficient equal to $1/2$.

b) diagrams, corresponding to the term $l_2(u_{3Q}u_Q^*v_{-Q} + v_{-3Q}v_{-Q}^*u_Q + h.c.)$. The combinatorial coefficient of all four is equal to $1/2$.

Diagrams **c)**, **d)**, **e)** are of the eighth order in u :

c) diagrams with a combinatorial coefficient of all four of them equal to 1. The upper two correspond to the term $l_3(|u_{3Q}|^2|u_Q|^2 + |v_{-3Q}|^2|v_{-Q}|^2)$, and the lower two correspond to the term $l_4(|u_{3Q}|^2|v_{-Q}|^2 + |v_{-3Q}|^2|u_Q|^2)$.

d) diagrams, corresponding to the term $l_5(u_{3Q}v_{-3Q}u_Q^*v_{-Q}^* + h.c.)$. The lower loop is a complex conjugate of the upper loop. The combinatorial coefficient is equal to 1.

e) diagrams, corresponding to the terms $l_6u_{3Q}u_Q^*v_{-Q}|u_Q|^2$ and $(l_7 + l_8)u_{3Q}u_Q^*v_{-Q}|v_{-Q}|^2$. There are even more loops which are complex conjugate to the ones shown on the picture, as well as loops obtained under the replacement $u \rightarrow v$. The values of such loops are the same, therefore we do not show them.

- (2002).
- ⁵ A. I. Larkin and Yu. N. Ovchinnikov, Zh. Eksp. Teor. Fiz. **47**, 1136 (1964) [Sov. Phys. JETP **20**, 762 (1965)].
 - ⁶ P. Fulde and R. A. Ferrel, Phys. Rev. **135**, A550 (1964).
 - ⁷ E. I. Rashba, Sov. Phys. - Solid State **2**, 1109 (1960).
 - ⁸ O. V. Dimitrova and M. V. Feigel'man, JETP Letters **78**, 637 (2003).
 - ⁹ H. Burkhardt and D. Rainer, Ann. Phys. (Berlin) **3**, 181 (1994).
 - ¹⁰ D. F. Agterberg, Physica C **387**, 13 (2003).
 - ¹¹ V. N. Popov, *Functional Integrals and Collective Excitations*, Cambridge University Press, Cambridge (1987).
 - ¹² V. P. Mineev, G. E. Volovik, Phys. Rev. B **18**, 3197 (1978).
 - ¹³ V. P. Mineev *Topologically Stable Defects and Solitons in Ordered Media*, Soviet Sc. Reviews, Sec A: Physics Reviews, V.2, ed. by I. M. Khalatnikov, Harwood Academic Publishers 1980; V. P. Mineev *Topologically Stable Defects and Solitons in Ordered Media* Harwood Academic Publishers 1998.
 - ¹⁴ M. M. Salomaa, G. E. Volovik, Rev. Mod. Phys. **59**, 533 (1987).
 - ¹⁵ T. H. R. Skyrme, Proc. Roy. Soc. (London) **260**, 127 (1961); **262**, 237 (1961); Nucl. Phys. **31**, 556 (1962).
 - ¹⁶ A.A.Belavin and A. M. Polyakov, Pis'ma ZhETF **22**, 503 (1975).
 - ¹⁷ G. E. Volovik and V. P. Mineev, Pis'ma ZhETF **24**, 605 (1976)[JETP Lett. **24**,561 (1976)]
 - ¹⁸ G. E. Volovik, Pis'ma ZhETF bf 70, 776 (1999) [JETP Letters **70**, 792 (1999)].
 - ¹⁹ D. A. Ivanov, Phys. Rev. Lett. **86**, 268 (2001).
 - ²⁰ S. K. Yip, Phys. Rev. B **65**, 144508 (2002).
 - ²¹ W. A. Little and R. D. Parks, Phys. Rev. Lett. **9**, 9 (1962).
 - ²² A. M. Polyakov, Phys. Lett. B, **59**, 79 (1975).
 - ²³ L. G. Aslamazov and A. I. Larkin, Phys. Lett. A **26**, 238 (1968); Sov. Phys. Solid State **10**, 875 (1968).
 - ²⁴ D. F. Agterberg and R. P. Kaur, cond-mat/0612216.